13. Liston, T. E., and L. J. Roberts, II. 1985. Transformation of prostaglandin D2 to 9 alpha, 11 beta-(15S)-trihydroxyprosta-(5Z,13E)-dien-1-oic acid (9 alpha, 11 beta-prostaglandin F2): a unique biologically active prostaglandin produced enzymatically in vivo in humans. *Proc. Natl. Acad. Sci. USA* 82: 6030–6034.
14. Beasley, C. R., C. Robinson, R. L. Featherstone, J. G. Varley, C. C. Hardy, M. K. Church, and S. T. Holgate. 1987. 9 alpha,11 beta-Prostaglandin F2, a novel metabolite of prostaglandin D2 is a potent contractile agonist of human and guinea pig airways. *J. Clin. Invest.* 79: 978–983.
15. Scher, J. U., and M. H. Pillinger. 2005. 15d-PGJ2: the anti-inflammatory prostaglandin? *Clin. Immunol.* 114: 100–109.
16. Forman, B. M., P. Tontonoz, J. Chen, R. P. Brun, B. M. Spiegelman, and R. M. Evans. 1995. 15-Deoxy-delta 12, 14-prostaglandin J2 is a ligand for the adipocyte determination factor PPAR gamma. *Cell* 83: 803–812.
17. Kliewer, S. A., J. M. Lenhard, T. M. Willson, I. Patel, D. C. Morris, and J. M. Lehmann. 1995. A prostaglandin J2 metabolite binds peroxisome proliferator-activated receptor gamma and promotes adipocyte differentiation. *Cell* 83: 813–819.
18. Ajuebor, M. N., A. Singh, and J. L. Wallace. 2000. Cyclooxygenase-2-derived prostaglandin D(2) is an early anti-inflammatory signal in experimental colitis. *Am. J. Physiol. Gastrointest. Liver Physiol.* 279: G238–G244.
19. Angeli, V., D. Staumont, A. S. Charbonnier, H. Hammad, P. Gosset, M. Pichavant, B. N. Lambrecht, M. Capron, D. Dombrowicz, and F. Trottein. 2004. Activation of the D prostanoid receptor 1 regulates immune and skin allergic responses. *J. Immunol.* 172: 3822–3829.
20. Monneret, G., S. Gravel, M. Diamond, J. Rokach, and W. S. Powell. 2001. Prostaglandin D2 is a potent chemoattractant for human eosinophils that acts via a novel DP receptor. *Blood* 98: 1942–1948.
21. Hammad, H., H. J. de Heer, T. Soullie, H. C. Hoogsteden, F. Trottein, and B. N. Lambrecht. 2003. Prostaglandin D2 inhibits airway dendritic cell migration and function in steady state conditions by selective activation of the D prostanoid receptor 1. *J. Immunol.* 171: 3936–3940.
22. Murata, T., K. Aritake, Y. Tsubosaka, T. Maruyama, T. Nakagawa, M. Hori, H. Hirai, M. Nakamura, S. Narumiya, Y. Urade, and H. Ozaki. 2013. Anti-inflammatory role of PGD2 in acute lung inflammation and therapeutic application of its signal enhancement. *Proc. Natl. Acad. Sci. USA* 110: 5205–5210.
23. Murata, T., M. I. Lin, K. Aritake, S. Matsumoto, S. Narumiya, H. Ozaki, Y. Urade, M. Hori, and W. C. Sessa. 2008. Role of prostaglandin D2 receptor DP as a suppressor of tumor hyperpermeability and angiogenesis in vivo. *Proc. Natl. Acad. Sci. USA* 105: 20009–20014.
24. Aritake, K., Y. Kado, T. Inoue, M. Miyano, and Y. Urade. 2006. Structural and functional characterization of HQL-79, an orally selective inhibitor of human hematopoietic prostaglandin D synthase. *J. Biol. Chem.* 281: 15277–15286.
25. Almishri, W., C. Cossette, J. Rokach, J. G. Martin, Q. Hamid, and W. S. Powell. 2005. Effects of prostaglandin D2, 15-deoxy-Delta12,14-prostaglandin J2, and selective DP1 and DP2 receptor agonists on pulmonary infiltration of eosinophils in Brown Norway rats. *J. Pharmacol. Exp. Ther.* 313: 64–69.
26. Spik, I., C. Brénuchon, V. Angéli, D. Staumont, S. Fleury, M. Capron, F. Trottein, and D. Dombrowicz. 2005. Activation of the prostaglandin D2 receptor DP2/CRTH2 increases allergic inflammation in mouse. *J. Immunol.* 174: 3703–3708.
27. Fujitani, Y., K. Aritake, Y. Kanaoka, T. Goto, N. Takahashi, K. Fujimori, and T. Kawada. 2010. Pronounced adipogenesis and increased insulin sensitivity caused by overproduction of prostaglandin D2 in vivo. *FEBS J.* 277: 1410–1419.
28. Satoh, T., R. Moroi, K. Aritake, Y. Urade, Y. Kanai, K. Sumi, H. Yokozeki, H. Hirai, K. Nagata, T. Hara, et al. 2006. Prostaglandin D2 plays an essential role in chronic allergic inflammation of the skin via CRTH2 receptor. *J. Immunol.* 177: 2621–2629.
29. Matsuoka, T., M. Hirata, H. Tanaka, Y. Takahashi, T. Murata, K. Kabashima, Y. Sugimoto, T. Kobayashi, F. Ushikubi, Y. Aze, et al. 2000. Prostaglandin D2 as a mediator of allergic asthma. *Science* 287: 2013–2017.
30. Murata, T., K. Aritake, S. Matsumoto, S. Kamauchi, T. Nakagawa, M. Hori, E. Momotani, Y. Urade, and H. Ozaki. 2011. Prostaglandin D2 is a mast cell-derived antiangiogenic factor in lung carcinoma. *Proc. Natl. Acad. Sci. USA* 108: 19802–19807.
31. Goetzl, E. J., and W. C. Pickett. 1981. Novel structural determinants of the human neutrophil chemotactic activity of leukotriene B. *J. Exp. Med.* 153: 482–487.
32. Kobayashi, K., Y. Tsubosaka, M. Hori, S. Narumiya, H. Ozaki, and T. Murata. 2013. Prostaglandin D2-DP signaling promotes endothelial barrier function via the cAMP/PKA/Tiam1/Rac1 pathway. *Arterioscler. Thromb. Vasc. Biol.* 33: 565–571.
33. Hirai, H., K. Tanaka, O. Yoshie, K. Ogawa, K. Kenmotsu, Y. Takamori, M. Ichimasa, K. Sugamura, M. Nakamura, S. Takano, and K. Nagata. 2001. Prostaglandin D2 selectively induces chemotaxis in T helper type 2 cells, eosinophils, and basophils via seven-transmembrane receptor CRTH2. *J. Exp. Med.* 193: 255–261.
34. Houle, F., and J. Huot. 2006. Dysregulation of the endothelial cellular response to oxidative stress in cancer. *Mol. Carcinog.* 45: 362–367.

nature immunology

Mast cell maturation is driven via a group III phospholipase A_2-prostaglandin D_2–DP1 receptor paracrine axis

Yoshitaka Taketomi[1,2], Noriko Ueno[1], Takumi Kojima[1], Hiroyasu Sato[1,2], Remi Murase[1,2], Kei Yamamoto[1], Satoshi Tanaka[3], Mariko Sakanaka[4], Masanori Nakamura[5], Yasumasa Nishito[6], Momoko Kawana[2], Naotomo Kambe[7], Kazutaka Ikeda[8], Ryo Taguchi[9], Satoshi Nakamizo[10], Kenji Kabashima[10], Michael H Gelb[11], Makoto Arita[12], Takehiko Yokomizo[13], Motonao Nakamura[14], Kikuko Watanabe[15], Hiroyuki Hirai[16], Masataka Nakamura[17], Yoshimichi Okayama[18], Chisei Ra[18], Kosuke Aritake[19], Yoshihiro Urade[19], Kazushi Morimoto[20], Yukihiko Sugimoto[20], Takao Shimizu[14], Shuh Narumiya[21], Shuntaro Hara[2] & Makoto Murakami[1]

Microenvironment-based alterations in phenotypes of mast cells influence the susceptibility to anaphylaxis, yet the mechanisms underlying proper maturation of mast cells toward an anaphylaxis-sensitive phenotype are incompletely understood. Here we report that PLA2G3, a mammalian homolog of anaphylactic bee venom phospholipase A_2, regulates this process. PLA2G3 secreted from mast cells is coupled with fibroblastic lipocalin-type PGD_2 synthase (L-PGDS) to provide PGD_2, which facilitates mast-cell maturation via PGD_2 receptor DP1. Mice lacking PLA2G3, L-PGDS or DP1, mast cell–deficient mice reconstituted with PLA2G3-null or DP1-null mast cells, or mast cells cultured with L-PGDS–ablated fibroblasts exhibited impaired maturation and anaphylaxis of mast cells. Thus, we describe a lipid-driven PLA2G3–L-PGDS–DP1 loop that drives mast cell maturation.

Anaphylaxis is a serious immediate allergic reaction that involves the activation of mast cells. Cross-linking of the high-affinity IgE receptor FcεRI on mast cells with IgE and antigen initiates signals leading to the release of allergic mediators that induce immediate hypersensitivity[1]. Anaphylaxis is triggered by allergens (for example, insect venom, food and medication) and damages multiple organs including the respiratory and circulatory systems, often leading to life-threatening episodes.

Environmentally induced alterations in phenotypes of mast cells could be one factor that influences the severity of anaphylaxis. Current evidence has established the essential role of stem cell factor (SCF) and its receptor c-Kit (CD117) for development of mast cells[2]. However, the SCF–c-Kit system alone is insufficient to drive the maturation of mast cells fully, as culture of immature mast cells with fibroblasts, but not with SCF alone, can induce differentiation into mature mast cells[2]. Although several cytokines, chemokines and adhesion molecules have supporting roles in tissue-specific homing, growth or differentiation of mast cells[3–7], precise mechanisms underlying mast cell–fibroblast communication leading to optimal maturation of mast cells still remain elusive.

Lipid mediators, such as prostaglandins, leukotrienes and lysophospholipids, have important roles in various biological processes, including allergy[8–15]. A given lipid mediator (for example, PGD_2) aggravates, suppresses or resolves allergic responses[11–13], and this functional variability may depend on the use of distinct biosynthetic enzyme and/or receptor subtypes in different cells. Eicosanoid biosynthesis is initiated by release of arachidonic acid from phospholipids by phospholipase A_2 (PLA_2) enzymes[16]. PLA2G4A (cytosolic PLA_2; $cPLA_2\alpha$) has an essential role in the generation of eicosanoids in various cells, and its deletion results in diminished airway hypersensitivity[17].

[1]Lipid Metabolism Project, Tokyo Metropolitan Institute of Medical Science, Tokyo, Japan. [2]School of Pharmacy, Showa University, Tokyo, Japan. [3]Department of Immunobiology, Okayama University Graduate School of Medicine, Dentistry and Pharmaceutical Sciences, Okayama, Japan. [4]School of Pharmacy and Pharmaceutical Sciences, Mukogawa Women's University, Hyogo, Japan. [5]School of Dentistry, Showa University, Tokyo, Japan. [6]Core Technology and Research Center, Tokyo Metropolitan Institute of Medical Science, Tokyo, Japan. [7]Department of Dermatology, Chiba University Graduate School of Medicine, Chiba, Japan. [8]Institute for Advanced Biosciences, Keio University, Yamagata, Japan. [9]College of Life and Health Sciences, Chubu University, Aichi, Japan. [10]Department of Dermatology, Kyoto University Graduate School of Medicine, Kyoto, Japan. [11]Departments of Chemistry and Biochemistry, University of Washington, Washington, USA. [12]Graduate School of Pharmaceutical Sciences, The University of Tokyo, Tokyo, Japan. [13]Department of Biochemistry, Juntendo University School of Medicine, Tokyo, Japan. [14]Faculty of Medicine, The University of Tokyo, Tokyo, Japan. [15]Department of Nutrition, Koshien University, Hyogo, Japan. [16]Department of Advanced Medicine and Development, Bio Medical Laboratories, Saitama, Japan. [17]Human Gene Sciences Center, Tokyo Medical and Dental University, Tokyo, Japan. [18]Division of Molecular Cell Immunology and Allergology, Advanced Medical Research Center, Nihon University Graduate School of Medical Science, Tokyo, Japan. [19]Department of Molecular Bihavioral Biology, Osaka Bioscience Institute, Osaka, Japan. [20]Department of Pharmaceutical Biochemistry, Graduate School of Medicine and Pharmaceutical Sciences, Kumamoto University, Kumamoto, Japan. [21]Department of Pharmacology, Kyoto University Graduate School of Medicine, Kyoto, Japan. Correspondence should be addressed to M.M. (murakami-mk@igakuken.or.jp).

Received 19 September 2012; accepted 11 March 2013; published online 28 April 2013; doi:10.1038/ni.2586

By contrast, the role of secreted PLA_2 ($sPLA_2$) enzymes is still a subject of debate. Although the lower asthmatic responses in mice lacking two classical $sPLA_2$ enzymes (PLA2G5 and PLA2G10) have revealed their contribution to asthma[18,19], the mechanisms underlying the actions of these enzymes remain poorly understood.

A major bee venom component responsible for anaphylaxis is an atypical form of $sPLA_2$ called BV-PLA_2[20,21]. The mammalian genome encodes group III $sPLA_2$ (PLA2G3), which is the sole homolog of BV-PLA_2[16,22–26]. Here we provide evidence that PLA2G3 is a major mast cell granule-associated $sPLA_2$ that facilitates the maturation of mast cells by driving a previously unrecognized lipid mediator circuit. PLA2G3 released from mast cells is coupled with fibroblast lipocalin-type PGD synthase (L-PGDS) to provide PGD_2, which then acts on type-1 PGD receptor, DP1, induced on mast cells to promote their maturation.

RESULTS

PLA2G3 is expressed in mast cells and induces their activation

When injected intradermally into the mouse ear pinnas, BV-PLA_2 or human PLA2G3 alone induced a similar, dose-dependent vascular leak and augmented passive cutaneous anaphylaxis (PCA) induced by IgE and antigen in $Kit^{+/+}$ mice but not in mast cell–deficient $Kit^{W\text{-}sh/W\text{-}sh}$ mice, in which the SCF receptor c-Kit has a substitution (**Fig. 1a,b**). The edema induced by PLA2G3 was accompanied by ultrastructural degranulation of dermal mast cells (**Fig. 1c**). PLA2G3 induced the release of histamine (**Fig. 1d**), but not of lactate dehydrogenase (**Supplementary Fig. 1a**), from mouse peritoneal mast cells (pMCs) in a Ca^{2+}-dependent manner, indicating that PLA2G3 elicits degranulation, not cell lysis.

Immunohistochemistry analysis revealed that PLA2G3 localized with toluidine blue$^+$ dermal mast cells in wild-type mice but not in $Pla2g3^{-/-}$ mice[22] (**Fig. 1e**). Punctate staining in resting mast cells and sparse staining in degranulated mast cells suggest that PLA2G3 is released upon degranulation (**Fig. 1e,f**). In bone marrow–derived cell populations, *Pla2g3* mRNA was more highly enriched in IL-3–driven bone marrow–derived mast cells (BMMCs) and thymic stromal lymphopoietin (TSLP)-driven bone marrow–derived basophils (BM basophils) than in GM-CSF–driven bone marrow–derived dendritic cells (BMDCs) and M-CSF–driven bone marrow–derived macrophages (BMDMs), and was undetectable in Swiss 3T3 fibroblasts (**Fig. 1g** and **Supplementary Fig. 1b**). Of the mRNAs encoding $sPLA_2$ isoforms, *Pla2g3* mRNA was expressed most abundantly in BMMCs, followed by *Pla2g5* and *Pla2g2e*, whereas mRNAs encoding the other $sPLA_2$ isoforms were undetectable, and SCF-fibroblast–driven maturation of these cells toward connective tissue mast cells (CTMCs) did not affect the expression of these $sPLA_2$ enzymes (**Supplementary Fig. 1c**). When we transfected rat mastocytoma RBL-2H3 cells with cDNA encoding PLA2G3 or a catalytically inactive PLA2G3 variant, III-HQ, in which the catalytic-center histidine was replaced with asparagine[23], release of β-hexosaminidase (β-HEX) and generation of PGD_2 induced by crosslinking of FcεRI by IgE and antigen (hereafter called IgE-Ag) was augmented in cells overexpressing native PLA2G3 but not catalytically inactive PLA2G3 (**Supplementary Fig. 1d**). Thus, PLA2G3 is the main $sPLA_2$ in mouse mast cells, is released by exocytosis and can augment activation of mast cells in a manner dependent upon its enzymatic activity.

Pla2g3 deletion ameliorates mast cell–associated anaphylaxis

Upon passive systemic anaphylaxis (PSA) induced by IgE-Ag, $Pla2g3^{+/+}$ and WBB6F1-$Kit^{+/+}$ mice, but not mast cell–deficient WBB6F1-$Kit^{W/W\text{-}v}$ mice, had much more plasma histamine and a temporary decrease in rectal temperature after systemic antigen challenge, whereas these responses were mild in $Pla2g3^{-/-}$ mice (**Fig. 2a**). Upon PCA induced by IgE-Ag (**Fig. 2b** and **Supplementary Fig. 1e**) or compound 48/80 (C48/80; **Fig. 2c**), edema was markedly lower in $Pla2g3^{-/-}$ mice than $Pla2g3^{+/+}$ mice. By contrast, transgenic overexpression of human

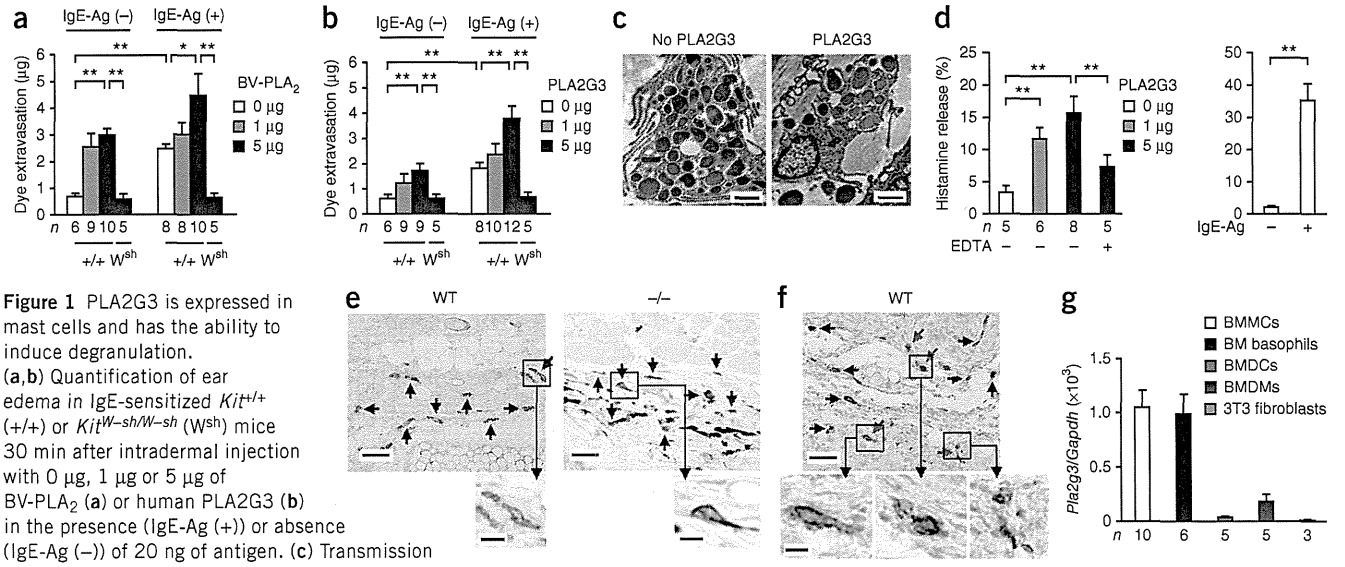

Figure 1 PLA2G3 is expressed in mast cells and has the ability to induce degranulation. (**a**,**b**) Quantification of ear edema in IgE-sensitized $Kit^{+/+}$ (+/+) or $Kit^{W\text{-}sh/W\text{-}sh}$ (W^{sh}) mice 30 min after intradermal injection with 0 μg, 1 μg or 5 μg of BV-PLA_2 (**a**) or human PLA2G3 (**b**) in the presence (IgE-Ag (+)) or absence (IgE-Ag (–)) of 20 ng of antigen. (**c**) Transmission electron microscopy of ear mast cells in wild-type mice with (+) or without (–) administration of 5 μg of PLA2G3. Scale bars, 2 μm. (**d**) Histamine release from wild-type mouse peritoneal cells after treatment for 30 min with 0 μg, 1 μg or 5 μg of PLA2G3 in the presence or absence of 2 mM EDTA (left). Histamine release by IgE-Ag stimulation (positive control) is also shown (right). (**e**,**f**) Immunohistochemistry analysis of ear-skin sections of wild-type (WT) or $Pla2g3^{-/-}$ (–/–) mice before (**e**) and 2 min after (**f**) stimulation with IgE-Ag with anti-PLA2G3 (α-PLA2G3), followed by counterstaining with toluidine blue (scale bars, 50 μm). Boxed areas are magnified below (scale bars, 5 μm). Blue and red arrows indicate resting and degranulated mast cells, respectively. (**g**) Real-time PCR of *Pla2g3* relative to *Gapdh* in indicated bone marrow–derived cells from wild-type mice and Swiss 3T3 fibroblasts. Data are from one experiment (**g**), and compiled from two (**d**) and three (**a**,**b**) experiments (mean ± s.e.m.; $*P < 0.05$ and $**P < 0.01$). Data in **c**,**e**,**f** are representative of two experiments.

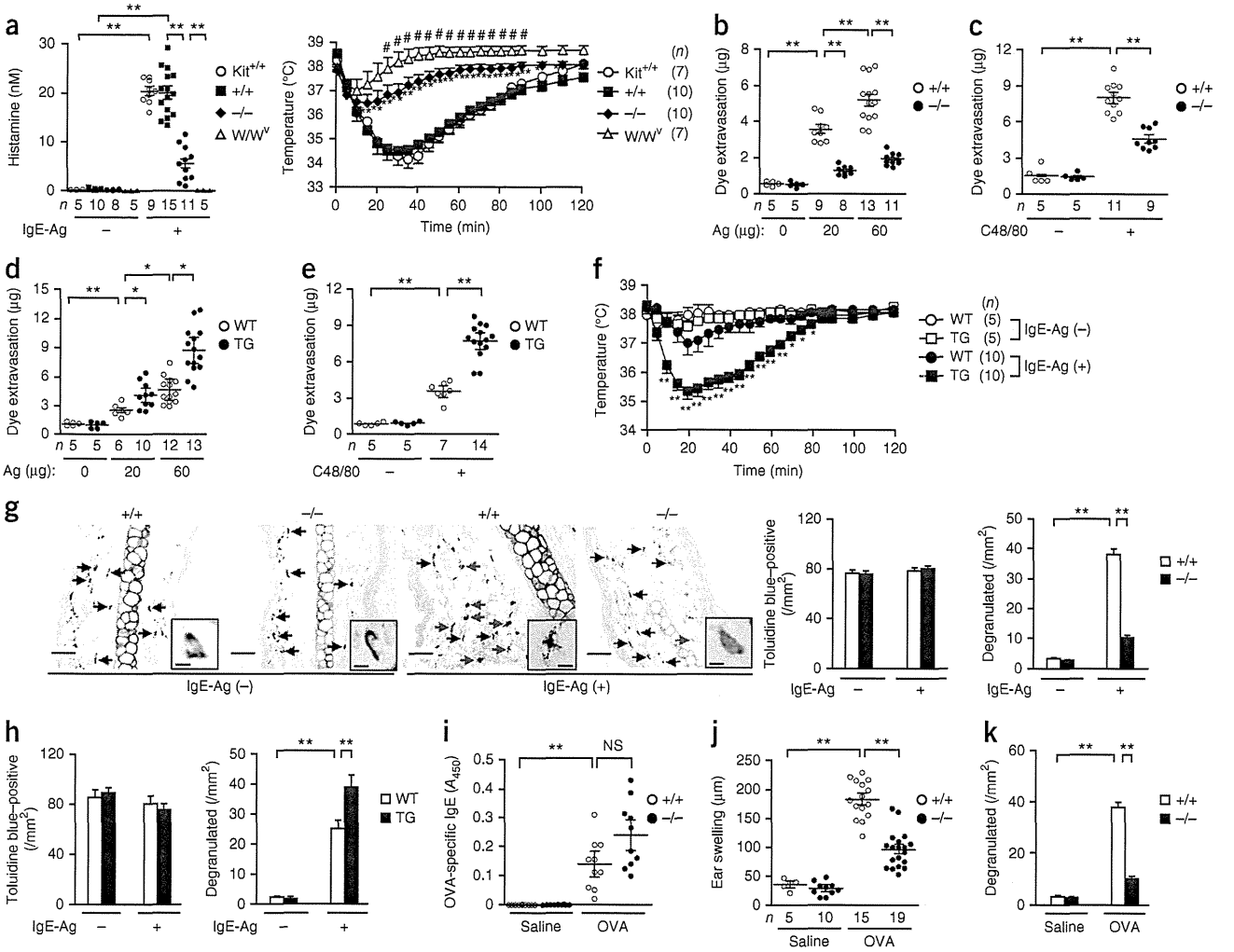

Figure 2 Altered anaphylaxis in mice with deletion or overexpression of PLA2G3. (**a**) Serum histamine concentrations (left) and rectal temperatures (right) in IgE-Ag–dependent PSA in *Pla2g3*$^{+/+}$ (+/+), *Pla2g3*$^{-/-}$ (–/–), WBB6F1-*Kit*$^{+/+}$ (Kit$^{+/+}$) and WBB6F1-*Kit*$^{W/W-v}$ (W/W^{v}) mice after challenge with 500 μg of antigen (Ag). $*P < 0.05$ and $**P < 0.01$, *Pla2g3*$^{-/-}$ versus *Pla2g3*$^{+/+}$ mice and $^{\#}P < 0.05$, *Kit*$^{W/W-v}$ versus *Pla2g3*$^{-/-}$ mice (right). (**b–e**) Analysis of ear edema in IgE-Ag–induced (**b**,**d**) or C48/80–induced (**c**,**e**) PCA in *Pla2g3*$^{+/+}$ (+/+) and *Pla2g3*$^{-/-}$ (–/–) mice (**b**,**c**) or wild-type (WT) and *PLA2G3*$^{tg/+}$ (TG) mice (**d**,**e**). (**f**) Rectal temperatures in IgE-Ag–dependent PSA in wild-type (WT) and *PLA2G3*$^{tg/+}$ (TG) mice after challenge with antigen (25 μg). $*P < 0.05$ and $**P < 0.01$, WT versus TG after antigen challenge. (**g**,**h**) Toluidine blue staining of skin sections (left) and counts of toluidine blue^{+} total and degranulated dermal mast cells (right) in *Pla2g3*$^{+/+}$ (+/+) and *Pla2g3*$^{-/-}$ (–/–) mice (**g**) or wild-type (WT) and *PLA2G3*$^{tg/+}$ (TG) mice (**h**) before (IgE-Ag (–)) and 2 min after (IgE-Ag (+)) IgE-Ag–mediated PCA (scale bars, 50 μm) ($n = 6$). Blue and red arrows indicate resting and degranulated mast cells, respectively (**g**). Insets, magnified images (scale bars, 5 μm) (**g**). (**i–k**) Serum levels of OVA-specific IgE ($n = 10$; **i**), ear swelling (**j**) and numbers of degranulated ear mast cells ($n = 6$; **k**) in OVA-induced active cutaneous anaphylaxis in *Pla2g3*$^{+/+}$ (+/+) and *Pla2g3*$^{-/-}$ (–/–) mice. Data are from one experiment (**f–i**,**k**) and compiled from three experiments (**a–e**,**j**) (mean ± s.e.m., $*P < 0.05$; $**P < 0.01$; NS, not significant).

PLA2G3 (*PLA2G3*$^{tg/+}$)[26] augmented both IgE-Ag–dependent (**Fig. 2d** and **Supplementary Fig. 1e**) and C48/80-induced (**Fig. 2e**) PCA as well as IgE-Ag–induced PSA (**Fig. 2f**). Although the ear skin of *Pla2g3*$^{-/-}$ and *Pla2g3*$^{+/+}$ mice contained an equivalent number of toluidine blue^{+} mast cells, we detected fewer cells showing signs of IgE-Ag–induced degranulation in *Pla2g3*$^{-/-}$ mice than in *Pla2g3*$^{+/+}$ mice (**Fig. 2g**). Conversely, ears of IgE-Ag–treated *PLA2G3*$^{tg/+}$ mice had more degranulated mast cells than those of replicate control mice despite a similar total mast cell count (**Fig. 2h**). IgE-Ag–induced PCA in mice lacking other sPLA$_2$ enzymes (*Pla2g2d*$^{-/-}$, *Pla2g2e*$^{-/-}$, *Pla2g2f*$^{-/-}$, *Pla2g5*$^{-/-}$ and *Pla2g10*$^{-/-}$) was similar to that in respective wild-type littermates (**Supplementary Fig. 1f**).

We immunized *Pla2g3*$^{+/+}$ and *Pla2g3*$^{-/-}$ mice intraperitoneally with alum-adsorbed ovalbumin (OVA) and elicited active cutaneous anaphylaxis by intradermal injection of OVA, which cross-links endogenous IgE-bound FcεRI on mast cells. Under conditions in which serum anti-OVA IgE levels were similar in both genotypes, *Pla2g3*$^{-/-}$ mice exhibited lower local anaphylaxis than did *Pla2g3*$^{+/+}$ mice, as indicated by notable reductions in ear swelling and mast cell degranulation (**Fig. 2i–k**). Thus, PLA2G3 is the sole sPLA$_2$ isoform associated with mast cell–dependent anaphylaxis.

Pla2g3 deletion impairs maturation of tissue mast cells

Transmission electron microscopy analysis revealed that resting mast cells in *Pla2g3*$^{+/+}$ mice were oval with regular short processes and had many secretory granules filled with electron-lucent and dense contents, whereas those in *Pla2g3*$^{-/-}$ mice had unusual granules that were small and irregular in size, suggesting the

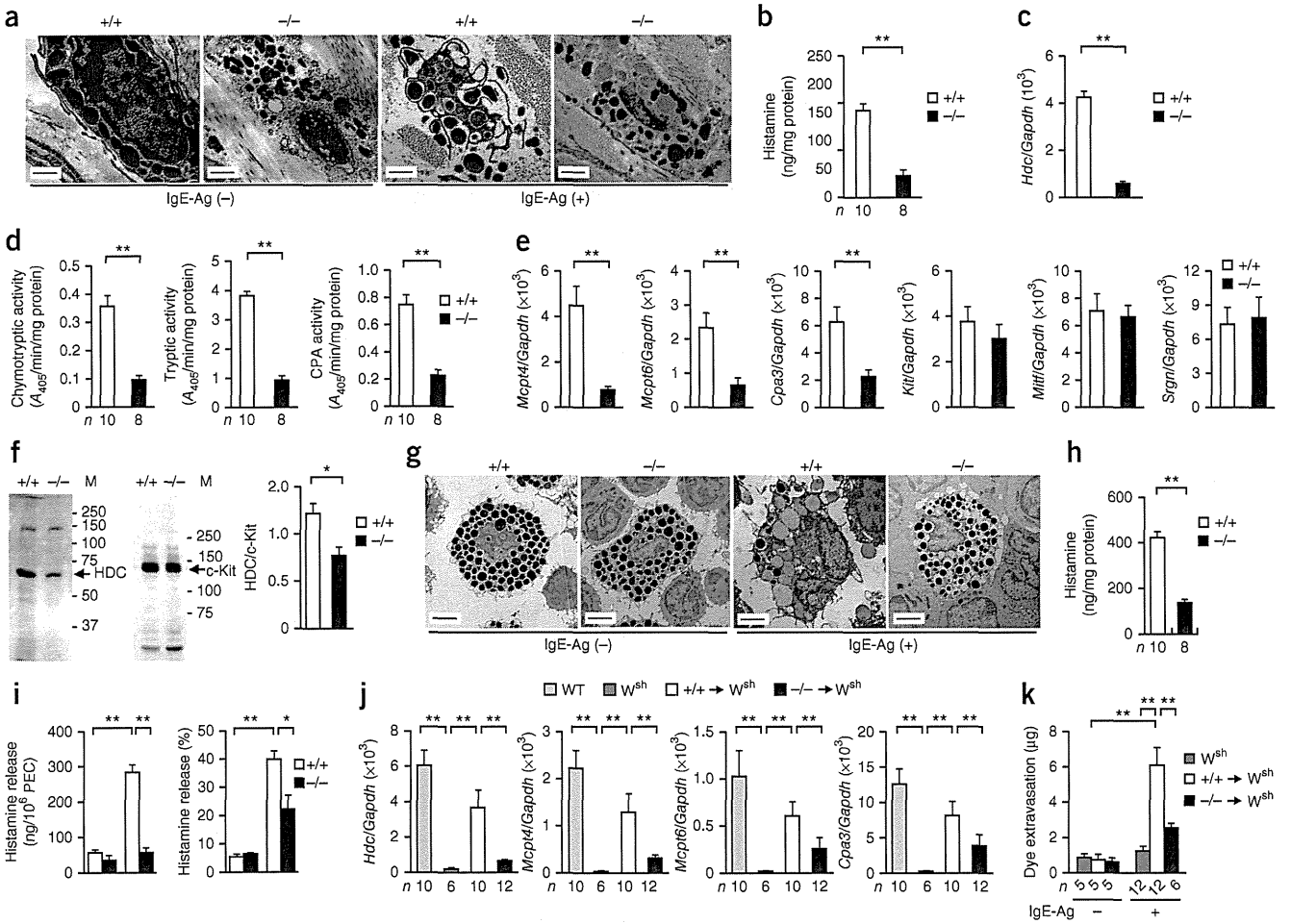

Figure 3 Immature properties of tissue mast cells in *Pla2g3*-deficient mice. (**a**) Transmission electron micrographs of ear mast cells in $Pla2g3^{+/+}$ (+/+) and $Pla2g3^{-/-}$ (−/−) mice before (IgE-Ag (−)) and 2 min after (IgE-Ag (+)) antigen (Ag) challenge. Scale bars, 2 μm. (**b**,**c**) Quantification of histamine amounts (**b**) and *Hdc* mRNA expression relative to that of *Gapdh* ($n = 12$; **c**) in ears of $Pla2g3^{+/+}$ (+/+) and $Pla2g3^{-/-}$ (−/−) mice. (**d**,**e**) Quantification of protease activity (**d**) and mRNA expression of mast cell proteases ($n = 12$) and other mast-cell markers ($n = 7$) (**e**) in ears of $Pla2g3^{+/+}$ (+/+) and $Pla2g3^{-/-}$ (−/−) mice. (**f**) Immunoblotting of HDC and c-Kit in ears of $Pla2g3^{+/+}$ (+/+) and $Pla2g3^{-/-}$ (−/−) mice. M, molecular mass (kDa). The ratio of HDC/c-Kit was quantified by densitometric analysis ($n = 4$). (**g**) Transmission electron micrographs of pMCs in $Pla2g3^{+/+}$ (+/+) and $Pla2g3^{-/-}$ (−/−) mice before (IgE-Ag (−)) and 2 min after (IgE-Ag (+)) stimulation with antigen. Scale bars, 2 μm. (**h**,**i**) Quantification of histamine content (**h**) and IgE-Ag–induced histamine release (quantity and percentage; **i**) in $Pla2g3^{+/+}$ (+/+) and $Pla2g3^{-/-}$ (−/−) pMCs. PEC, peritoneal cells. (**j**,**k**) Expression of mast-cell marker mRNAs (**j**) and dye extravasation in IgE-Ag–dependent PCA (**k**) in ears of $Pla2g3^{+/+}$ (+/+) or $Pla2g3^{-/-}$ (−/−) BMMC-reconstituted or nonreconstituted $Kit^{W\text{-}sh/W\text{-}sh}$ (W^{sh}) mice and wild-type (WT) $Kit^{+/+}$ mice. Data are compiled from two (**d**,**h**,**i**) or three (**b**,**c**,**e**,**j**,**k**) experiments (mean ± s.e.m., $*P < 0.05$; $**P < 0.01$). Images are representative of one (**f**) or two (**a**,**g**) experiments.

immaturity of mast cells (**Fig. 3a** and **Supplementary Fig. 2a**). After challenge with antigen, $Pla2g3^{+/+}$ skin mast cells exhibited features typical of degranulation, whereas $Pla2g3^{-/-}$ mast cells were almost insensitive. In agreement, the amount of histamine (**Fig. 3b**) and the expression of *Hdc* (which encodes histidine decarboxylase, a histamine-biosynthetic enzyme; **Fig. 3c**) were lower in the ears of $Pla2g3^{-/-}$ mice than in those of $Pla2g3^{+/+}$ mice. Enzymatic activity (**Fig. 3d**) and expression (**Fig. 3e**) of mast cell proteases, including chymase (encoded by *Mcpt4*), tryptase (encoded by *Mcpt6*) and carboxypeptidase (encoded by *Cpa3*), were also notably lower in the ears of $Pla2g3^{-/-}$ mice relative to $Pla2g3^{+/+}$ mice. However, expression of *Kit*, *Mitf* (which encodes a transcription factor essential for mast cell differentiation) and *Srgn* (which encodes serglycin, a proteoglycan core protein) was unchanged in ears of $Pla2g3^{-/-}$ mice (**Fig. 3e**), indicating that not all mast cell markers were affected by PLA2G3 deficiency. We confirmed the lower expression of HDC and the unaltered expression of c-Kit in the skin of $Pla2g3^{-/-}$ mice by immunoblotting (**Fig. 3f**).

$Pla2g3^{-/-}$ pMCs also had smaller and more irregular granules (**Fig. 3g** and **Supplementary Fig. 2b**), contained less histamine (**Fig. 3h**) and exhibited less IgE-Ag–induced histamine release (both amount and percentage; **Fig. 3i**) than $Pla2g3^{+/+}$ pMCs. Although the proportion of $Kit^{+}Fc\varepsilon RI\alpha^{+}$ skin mast cells or pMCs was similar in both genotypes, surface expression of FcεRIα was lower in $Pla2g3^{-/-}$ mice than in $Pla2g3^{+/+}$ mice (**Supplementary Fig. 2c**,**d**). A23187-induced histamine release by $Pla2g3^{-/-}$ pMCs was lower in terms of amount, but not percentage, compared to that by $Pla2g3^{+/+}$ pMCs (**Supplementary Fig. 2e**), suggesting that the attenuated IgE-Ag–induced degranulation and anaphylaxis in $Pla2g3^{-/-}$ mice was mainly due to the lower histamine content and surface FcεRI expression. Furthermore, intestinal expression of *Mcpt1* and *Mcpt2* (which encode mucosal mast-cell proteases) was markedly

lower in *Pla2g3*$^{-/-}$ mice than in *Pla2g3*$^{+/+}$ mice (**Supplementary Fig. 2f**). Thus, the lower anaphylaxis in *Pla2g3*$^{-/-}$ mice may result from abnormalities in the maturation and degranulation of mast cells in multiple anatomical sites. Other immune-cell populations in the skin and spleen were unaffected by PLA2G3 deficiency (**Supplementary Fig. 2g,h**).

To assess whether the aberrant features of mast cells in *Pla2g3*$^{-/-}$ mice relied on the absence of PLA2G3 in the mast cells themselves or in mast cell microenvironment, we transferred *Pla2g3*$^{+/+}$ or *Pla2g3*$^{-/-}$ BMMCs intradermally into mast cell–deficient *Kit*$^{W\text{-}sh/W\text{-}sh}$ mice. After 6 weeks, the distribution of mast cells in the ear dermis was comparable between mice reconstituted with *Pla2g3*$^{+/+}$ BMMCs and those reconstituted with *Pla2g3*$^{-/-}$ BMMCs (**Supplementary Fig. 3a**). Expression of mast-cell marker genes *Hdc*, *Mcpt4*, *Mcpt6* and *Cpa3* (**Fig. 3j**) and IgE-Ag–mediated PCA (**Fig. 3k** and **Supplementary Fig. 3b**) was much greater in the ears of mice that received *Pla2g3*$^{+/+}$ BMMCs over control *Kit*$^{W\text{-}sh/W\text{-}sh}$ mice, whereas these changes were scarcely seen in mice that received *Pla2g3*$^{-/-}$ BMMCs. We observed similar results when we transferred *Pla2g3*$^{+/+}$ or *Pla2g3*$^{-/-}$ BMMCs intravenously into *Kit*$^{W\text{-}sh/W\text{-}sh}$ mice. After 12 weeks of reconstitution, IgE-Ag–mediated PCA was restored in mice reconstituted with *Pla2g3*$^{+/+}$ BMMCs but remained poor in mice reconstituted with *Pla2g3*$^{-/-}$ BMMCs, although we observed similar numbers of reconstituted mast cells in the ear dermis (**Supplementary Fig. 3c,d**). In these experiments, low levels of mast-cell engraftment in the skin of *Kit*$^{W\text{-}sh/W\text{-}sh}$ mice relative to baseline amounts in the skin of wild-type mice restored PCA efficiently. *Kit*$^{W\text{-}sh/W\text{-}sh}$ mice transferred with *PLA2G3*$^{tg/+}$ BMMCs had a greater PCA response compared to those transferred with control BMMCs (**Supplementary Fig. 3e**). Altogether, the defective maturation and activation of mast cells in *Pla2g3*$^{-/-}$ mice are cell autonomous, even though the migration of mast cell progenitors into extravasuclar tissues is not profoundly impaired by PLA2G3 deficiency.

Impaired maturation of *Pla2g3*$^{-/-}$ mast cells in culture

Pla2g3$^{-/-}$ BMMCs grew normally in medium supplemented with IL-3 (**Supplementary Fig. 4a**) and, unlike tissue-resident mast cells, they had normal surface expression of FcεRIα (**Supplementary Fig. 4b**). Stimulation with IgE-Ag induced a robust release of $sPLA_2$ activity from wild-type BMMCs, whereas this release was ablated in *Pla2g3*$^{-/-}$ BMMCs and augmented in *PLA2G3*$^{tg/+}$ BMMCs (**Supplementary Fig. 4c,d**), confirming that PLA2G3 is released upon degranulation. IgE-Ag–stimulated *Pla2g3*$^{-/-}$ BMMCs released less histamine, PGD_2 and LTC_4 than *Pla2g3*$^{+/+}$ BMMCs, whereas these responses were greater in *PLA2G3*$^{tg/+}$ BMMCs than in control BMMCs (**Supplementary Fig. 4e–j**). IgE-Ag–induced influx of Ca^{2+}, induction of cytokines (encoded by *Il4, Il6* and *Tnf*) and phosphorylation of phospholipase C (PLCγ2) and Akt were similar between the genotypes (**Supplementary Fig. 4k–m**), suggesting that FcεRI-dependent signaling was not profoundly perturbed by PLA2G3 deficiency. Generation of eicosanoids by mast cells depends on $cPLA_2\alpha$, which is regulated by Ca^{2+}-dependent membrane translocation and MAP kinase-directed phosphorylation[17]. Consistent with the lower generation of eicosanoids (**Supplementary Fig. 4f,g**), FcεRI-dependent phosphorylation of ERK (not JNK and p38) and $cPLA_2\alpha$ and decrease in arachidonic acid–containing phosphatidylcholine were partially impaired in *Pla2g3*$^{-/-}$ BMMCs compared to *Pla2g3*$^{+/+}$ BMMCs, despite the equivalent expression of total ERK and $cPLA_2\alpha$ proteins in both cells (**Supplementary Fig. 4m–o**). Thus, PLA2G3 deficiency attenuates activation of ERK and $cPLA_2\alpha$ in BMMCs.

We took advantage of an *in vitro* system in which immature BMMCs undergo maturation toward mature CTMC-like cells in coculture with Swiss 3T3 fibroblasts[27]. PLA2G3 deficiency did not affect the proliferation of BMMCs in coculture (**Supplementary Fig. 5a**). During coculture, $sPLA_2$ activity was secreted from wild-type BMMCs in response to SCF, whereas $sPLA_2$ secretion was absent in *Pla2g3*$^{-/-}$ BMMCs and augmented in *PLA2G3*$^{tg/+}$ BMMCs (**Fig. 4a,b**). Although the ultrastructure of *Pla2g3*$^{-/-}$ BMMCs appeared normal, *Pla2g3*$^{-/-}$ CTMC-like cells contained unusual granules with less electron-dense contents than did *Pla2g3*$^{+/+}$ CTMC-like cells (**Fig. 4c** and **Supplementary Fig. 5b**). After coculture, the expression of *Hdc* (**Fig. 4d**) and its product histamine (**Fig. 4e**) were markedly greater in *Pla2g3*$^{+/+}$ CTMC-like cells, whereas these changes were barely seen in *Pla2g3*$^{-/-}$ cells. Even before coculture, *Hdc* expression and histamine content were slightly lower in *Pla2g3*$^{-/-}$ BMMCs than in *Pla2g3*$^{+/+}$ BMMCs, indicating that some early developmental process had already been perturbed by PLA2G3 deficiency. IgE-Ag–induced histamine release was greater in *Pla2g3*$^{+/+}$ cells after coculture than before coculture, whereas this coculture-driven increase in histamine release was impaired in *Pla2g3*$^{-/-}$ cells (**Fig. 4f**). Conversely, coculture-induced *Hdc* expression was greater in *PLA2G3*$^{tg/+}$ CTMC-like cells than in control cells (**Supplementary Fig. 5c**). Supplementation with PLA2G3 in coculture significantly restored the histamine level in *Pla2g3*$^{-/-}$ CTMC-like cells and also elevated it in *Pla2g3*$^{+/+}$ cells (**Fig. 4g**). *Pla2g3*$^{-/-}$ BMMCs without coculture did not respond to PLA2G3 (**Fig. 4g**), suggesting that the action of PLA2G3 on histamine synthesis in mast cells depends on fibroblasts. Histamine content in *Pla2g3*$^{+/+}$ BMMCs without coculture was substantially lower in the presence of PLA2G3 than its absence (**Fig. 4g**), which might reflect that the enzyme elicits the release of prestored histamine by degranulation (**Fig. 1b**).

The maturation of wild-type BMMCs to CTMC-like cells increased FcεRI-dependent PGD_2 synthesis (**Fig. 4h**), with a concomitant increase in *Ptgds2* (hematopoietic PGD_2 synthase; H-PGDS) (**Fig. 4i**). However, these changes in the PGD_2 pathway occurred only weakly in *Pla2g3*$^{-/-}$ cells. Surface expression of FcεRIα was significantly elevated in *Pla2g3*$^{+/+}$ cells but not in *Pla2g3*$^{-/-}$ cells after coculture (**Supplementary Fig. 5d**), consistent with the lower surface FcεRIα expression on tissue-resident mast cells in *Pla2g3*$^{-/-}$ mice. The coculture-driven induction of *Mcpt4* and *Mcpt6* (which encode mast cell proteases) and *Ndrg1* (which encodes a mast cell granule–associated protein[27]) was also impaired in *Pla2g3*$^{-/-}$ cells, whereas the constitutive expression of *Srgn* and *Kit* was unaffected (**Supplementary Fig. 5e**). We verified the attenuated induction of HDC and H-PGDS and the unaltered expression of c-Kit in *Pla2g3*$^{-/-}$ CTMC-like cells at the protein level (**Fig. 4j**). Although *Pla2g3*$^{+/+}$ CTMC-like cells acquired sensitivity to C48/80 after coculture[27], C48/80-induced degranulation (**Fig. 4k**) and induction of the putative C48/80 receptors encoded by *Mrgprx1* and *Mrgprx2* (ref. 28; **Supplementary Fig. 5e**) after coculture were lower in *Pla2g3*$^{-/-}$ cells. The coculture-dependent decrease in *Itga5* (which encodes integrin α_E) and increase in *Icam1* (which encodes integrin β_7), which participates in tissue homing of mast-cell progenitors[6], were unaffected by PLA2G3 deficiency (**Supplementary Fig. 5e**), consistent with the unaltered number of mast cells in *Pla2g3*$^{-/-}$ tissues. Microarray gene profiling using *Pla2g3*$^{+/+}$ and *Pla2g3*$^{-/-}$ BMMCs before and after coculture revealed that, of the ~41,000 genes examined, *Pla2g3*$^{+/+}$ cells expressed 3,632 coculture-inducible genes, of which 1,409 genes were barely or only partially induced in *Pla2g3*$^{-/-}$ cells. Genes affected by *Pla2g3* ablation included, for example, genes associated with secretory granules, genes related to biosynthesis or receptors for lipid mediators,

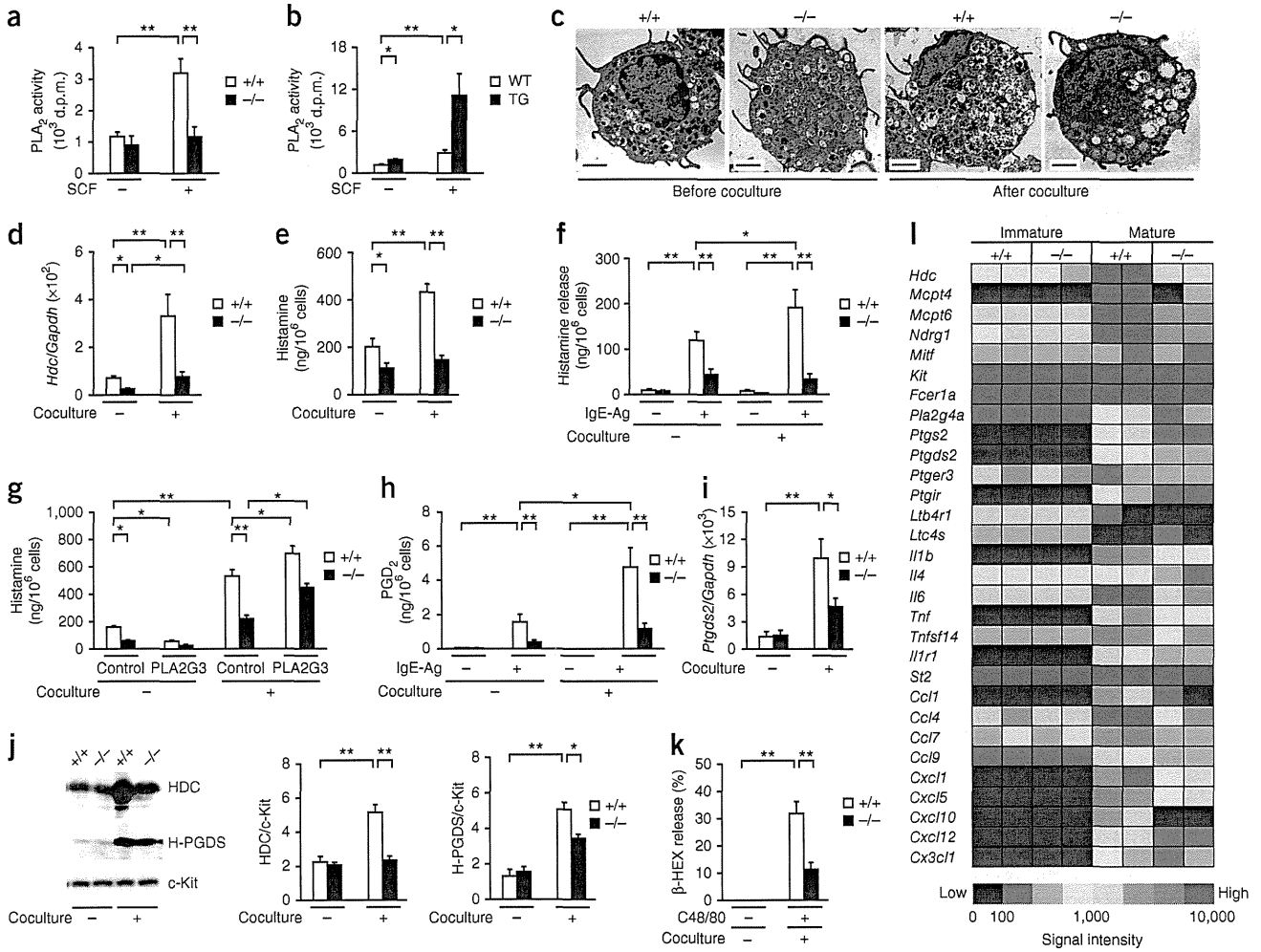

Figure 4 Defective fibroblast-driven maturation of *Pla2g3*$^{-/-}$ BMMCs. (**a**,**b**) Release of sPLA$_2$ activity from *Pla2g3*$^{+/+}$ (+/+) and *Pla2g3*$^{-/-}$ (−/−) BMMCs (**a**) or from *PLA2G3*$^{tg/+}$ (TG) and wild-type (WT) BMMCs (**b**) with or without 100 ng/ml SCF for 30 min ($n = 4$). d.p.m., disintegrations per minute. (**c**) Transmission electron microscopy of *Pla2g3*$^{+/+}$ (+/+) and *Pla2g3*$^{-/-}$ (−/−) BMMCs before and on day 4 of coculture with Swiss 3T3 fibroblasts. Scale bars, 2 μm. (**d**–**k**) Expression of *Hdc* relative to *Gapdh* ($n = 8$; **d**), cellular histamine levels ($n = 8$; **e**), histamine release with (IgE-Ag (+)) or without (IgE-Ag (−)) antigen challenge ($n = 8$; **f**), cellular histamine levels after culture in the presence or absence (control) of 2 μg/ml human PLA2G3 ($n = 6$; **g**), PGD$_2$ generation with or without antigen challenge ($n = 8$; **h**), *Ptgds2* expression ($n = 8$; **i**), immunoblot of HDC ($n = 6$) and H-PGDS ($n = 3$) relative to c-Kit (**j**) and C48/80-induced β-HEX release ($n = 7$; **k**) in *Pla2g3*$^{+/+}$ (+/+) or *Pla2g3*$^{-/-}$ (−/−) BMMCs before (−) and on day 4 of (+) coculture. (**l**) Microarray gene profile of *Pla2g3*$^{+/+}$ (+/+) and *Pla2g3*$^{-/-}$ (−/−) BMMCs before immature and on day 4 of mature coculture. Results from duplicate experiments are shown (columns). Heat maps are globally normalized for all genes. Data are from one experiment (**a**,**b**,**l**) and compiled from two (**d**,**e**,**g**,**j**,**k**) or three (**f**,**h**,**i**) experiments (mean ± s.e.m., $*P < 0.05$; $**P < 0.01$). Images in **c** are representative of two experiments.

and genes for cytokines, chemokines and their receptors (**Fig. 4l** and **Supplementary Table 1**), underscoring the immaturity of *Pla2g3*$^{-/-}$ cells, particularly after coculture.

By comparison, *Pla2g4a*$^{-/-}$ mice exhibited normal IgE-Ag–induced PCA, with normal counts of dermal mast cells and normal amounts of histamine (**Supplementary Fig. 5f–h**). IgE-Ag–induced histamine release, cellular histamine content and *Hdc* expression were unaffected by ablation of cPLA$_2$α (**Supplementary Fig. 5i–k**). Neither PGD$_2$ nor LTC$_4$ was produced by *Pla2g4a*$^{-/-}$ BMMCs (**Supplementary Fig. 5l,m**), confirming the obligatory role of cPLA$_2$α in eicosanoid synthesis in mast cells[29]. Thus, the absence of mast cell–derived eicosanoids by cPLA$_2$α deficiency did not affect maturation, degranulation and anaphylaxis of mast cells, suggesting that the effect of PLA2G3 deficiency on mast cells could not be simply explained by defective synthesis of eicosanoids by mast cells.

PGD$_2$-DP1 signals mast-cell maturation downstream of PLA2G3

To identify the specific lipid-mediator pathway that lies downstream of PLA2G3, we induced IgE-Ag–dependent PCA on mouse lines deficient in various eicosanoid receptors or biosynthetic enzymes. Of the eicosanoid receptor–deficient mouse lines tested, PCA was lower only in mice lacking the PGD receptor DP1 (*Ptgdr*$^{-/-}$)[9]. Vascular leakage was lower and ear mast cells exhibited poor degranulation despite an unaltered total count in *Ptgdr*$^{-/-}$ mice compared to wild-type mice (**Fig. 5a,b**). Dermal mast cells in *Ptgdr*$^{-/-}$ mice had fewer mature secretory granules, contained less histamine and were less sensitive to IgE-Ag–induced degranulation than those in *Ptgdr*$^{+/+}$ mice (**Fig. 5c,d**). Whereas the PCA was efficiently restored in *Kit*$^{W\text{-}sh/W\text{-}sh}$ mice reconstituted with *Ptgdr*$^{+/+}$ BMMCs, it was restored only partially in those mice reconstituted with *Ptgdr*$^{-/-}$ BMMCs (**Fig. 5e**). The PCA was unaltered or only slightly augmented in mice lacking other

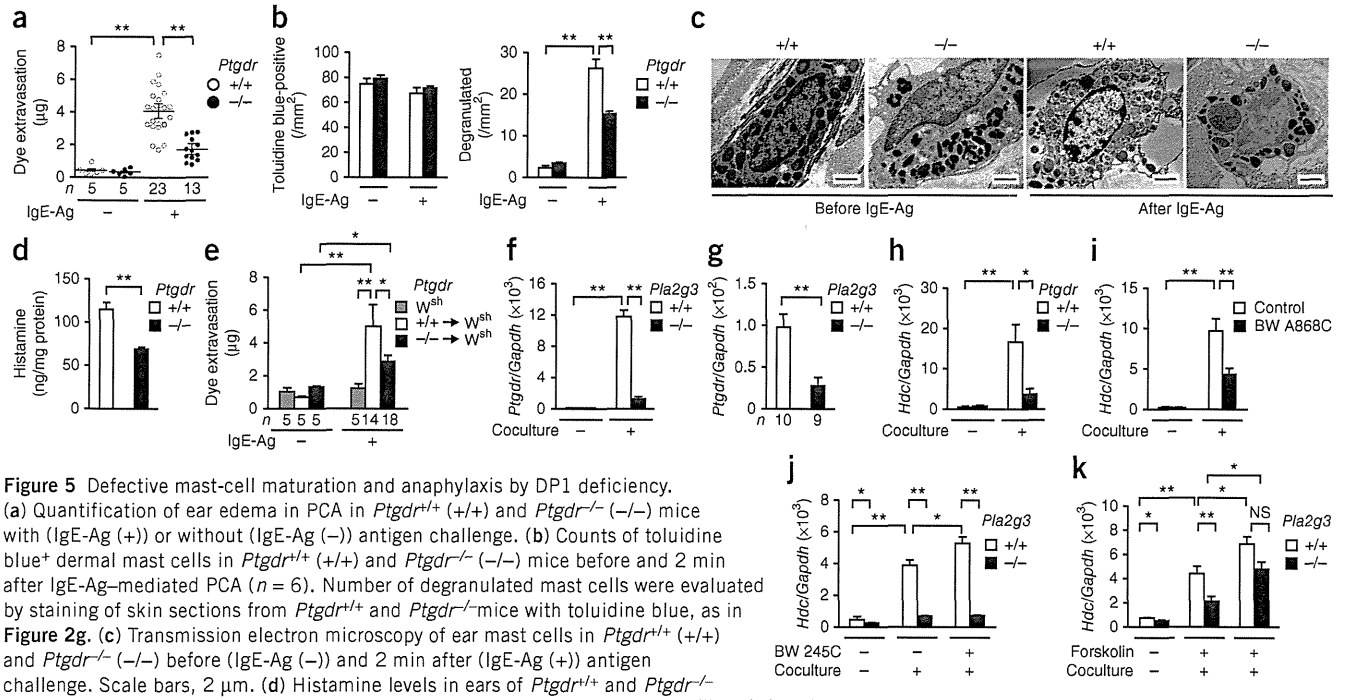

Figure 5 Defective mast-cell maturation and anaphylaxis by DP1 deficiency. (**a**) Quantification of ear edema in PCA in *Ptgdr*$^{+/+}$ (+/+) and *Ptgdr*$^{-/-}$ (−/−) mice with (IgE-Ag (+)) or without (IgE-Ag (−)) antigen challenge. (**b**) Counts of toluidine blue^{+} dermal mast cells in *Ptgdr*$^{+/+}$ (+/+) and *Ptgdr*$^{-/-}$ (−/−) mice before and 2 min after IgE-Ag–mediated PCA ($n = 6$). Number of degranulated mast cells were evaluated by staining of skin sections from *Ptgdr*$^{+/+}$ and *Ptgdr*$^{-/-}$mice with toluidine blue, as in **Figure 2g**. (**c**) Transmission electron microscopy of ear mast cells in *Ptgdr*$^{+/+}$ (+/+) and *Ptgdr*$^{-/-}$ (−/−) before (IgE-Ag (−)) and 2 min after (IgE-Ag (+)) antigen challenge. Scale bars, 2 μm. (**d**) Histamine levels in ears of *Ptgdr*$^{+/+}$ and *Ptgdr*$^{-/-}$ mice ($n = 10$). (**e**) Quantification of ear edema in IgE-Ag–dependent PCA in *Kit*$^{W\text{-}sh/W\text{-}sh}$ (W^{sh}) mice with or without reconstitution with *Ptgdr*$^{+/+}$ (+/+) or *Ptgdr*$^{-/-}$ (−/−) BMMCs. (**f**,**g**) Expression of *Ptgdr* in *Pla2g3*$^{+/+}$ and *Pla2g3*$^{-/-}$ BMMCs before and on day 2 of coculture ($n = 6$; **f**) and in the ear of *Pla2g3*$^{+/+}$ and *Pla2g3*$^{-/-}$ mice (**g**). (**h**,**i**) Expression of *Hdc* relative to *Gapdh* in *Ptgdr*$^{+/+}$ and *Ptgdr*$^{-/-}$ BMMCs ($n = 6$; **h**) or in wild-type BMMCs with or without BW A868C ($n = 7$; **i**) before and on day 2 of coculture. (**j**,**k**) Expression of *Hdc* relative to *Gapdh* in *Pla2g3*$^{+/+}$ and *Pla2g3*$^{-/-}$ BMMCs before and on day 2 of coculture with or without BW 245C ($n = 6$; **j**) or forskolin ($n = 6$; **k**). Data are compiled from two (**b**,**d**,**f**–**k**) or three (**a**,**e**) experiments (mean ± s.e.m., $^{*}P < 0.05$; $^{**}P < 0.01$; NS, not significant). Images in **c** are representative of two experiments.

eicosanoid receptors or biosynthetic enzymes (*Ptgdr2*$^{-/-}$, *Ptger1*$^{-/-}$, *Ptger2*$^{-/-}$, *Ptger3*$^{-/-}$, *Ptger4*$^{-/-}$, *Ptgfr*$^{-/-}$, *Ptgir*$^{-/-}$, *Tbxa2r*$^{-/-}$, *Ltb4r1*$^{-/-}$, *Ltb4r2*$^{-/-}$, *Ptges*$^{-/-}$, *Ptges2*$^{-/-}$ and *Alox15*$^{-/-}$; **Supplementary Fig. 6a**). Although *Ltc4s*$^{-/-}$ mice exhibited a lower PCA response as reported[10], their ear histamine content was unaffected (data not shown). Thus, abnormalities in mast cells observed in mice lacking PLA2G3 were phenocopied only in mice lacking DP1.

Next we examined the expression and function of DP1 in a mast cell–fibroblast coculture system[27]. Although we barely detected *Ptgdr* mRNA in BMMCs and Swiss 3T3 fibroblasts, *Ptgdr* mRNA was robustly induced in *Pla2g3*$^{+/+}$, but not in *Pla2g3*$^{-/-}$, CTMC-like cells after coculture (**Fig. 5f**). Consistently, *Ptgdr* expression in the ear was lower in *Pla2g3*$^{-/-}$ mice than in *Pla2g3*$^{+/+}$ mice (**Fig. 5g**). In agreement with the lower histamine amount in *Ptgdr*$^{-/-}$ dermal mast cells (**Fig. 5d**), the coculture-driven *Hdc* induction was severely impaired in *Ptgdr*$^{-/-}$ CTMC-like cells (**Fig. 5h**). In addition, the DP1 antagonist BW A868C prevented the coculture-induced upregulation of *Hdc* in wild-type CTMC-like cells (**Fig. 5i**). Conversely, the DP1 agonist BW 245C significantly enhanced *Hdc* induction in wild-type CTMC-like cells (**Fig. 5j**). However, the coculture-driven *Hdc* expression was barely restored by BW 245C in *Pla2g3*$^{-/-}$ mice (**Fig. 5j**), likely because DP1 induction was blunted by PLA2G3 deficiency (**Fig. 5f**). To circumvent this problem, we used the cAMP-elevating agent forskolin because DP1 is coupled with Gs-cAMP signaling[9]. The addition of forskolin to the coculture bypassed the requirement for DP1 in the induction of *Hdc* in *Pla2g3*$^{-/-}$ CTMC-like cells (**Fig. 5k**). By comparison, the expression of *Ptgdr2*, which encodes another PGD_2 receptor known as CRTH2, was high in BMMCs and lowered in accordance with their maturation into CTMC-like cells, without being affected by the *Pla2g3* genotypes (**Supplementary Fig. 6b**). Moreover, *Hdc* induction in CTMC-like cells was unaffected by CRTH2 deficiency in coculture, and *Ptgdr2* expression was unaffected by PLA2G3 deficiency *in vivo* (**Supplementary Fig. 6c,d**). The coculture-driven production of other eicosanoids such as 15-HETE and PGI_2 was unaffected by PLA2G3 deficiency (**Supplementary Fig. 6e**). Thus, DP1-cAMP signaling is specifically required for the PLA2G3-dependent maturation of mast cells.

L-PGDS supplies a PGD_2 pool for mast-cell maturation

We hypothesized that the absence of PGD_2 biosynthetic enzyme(s), acting downstream of PLA2G3 and upstream of DP1, would also influence maturation of mast cells. Of the two PGD_2 synthase–encoding genes, *Ptgds2* (which encodes H-PGDS) was expressed in BMMCs but not in Swiss 3T3 fibroblasts, whereas *Ptgds* (which encodes lipocalin-type PGDS; L-PGDS) expression was higher in fibroblasts than in BMMCs (**Fig. 6a**) and was below the detection limit in pMCs (data not shown). L-PGDS immunoreactivity was associated with fibroblasts surrounding toluidine blue^{+} mast cells in mouse skin (**Supplementary Fig. 7a**). PCA was exacerbated in *Ptgds2*$^{-/-}$ mice[30], which lack H-PGDS (**Fig. 6b**), whereas it was suppressed in *Ptgds*$^{-/-}$ mice[31], which lack L-PGDS (**Fig. 6c**), in comparison with respective control mice. *Ptgds*$^{-/-}$ mice had fewer degranulated ear mast cells than did *Ptgds*$^{+/+}$ mice after antigen challenge, although the total mast cell count was unaffected (**Fig. 6d**). Dermal mast cells in *Ptgds*$^{-/-}$ mice were ultrastructurally immature (that is, cytoplasmic granules were small and heterogeneous), comparatively resistant to antigen-induced degranulation, and contained less histamine than those in *Ptgds*$^{+/+}$ mice (**Fig. 6e,f**). Thus, the notable similarity among *Pla2g3*$^{-/-}$, *Ptgds*$^{-/-}$ and *Ptgdr*$^{-/-}$ mice suggests that PLA2G3, L-PGDS and DP1 may lie in the same

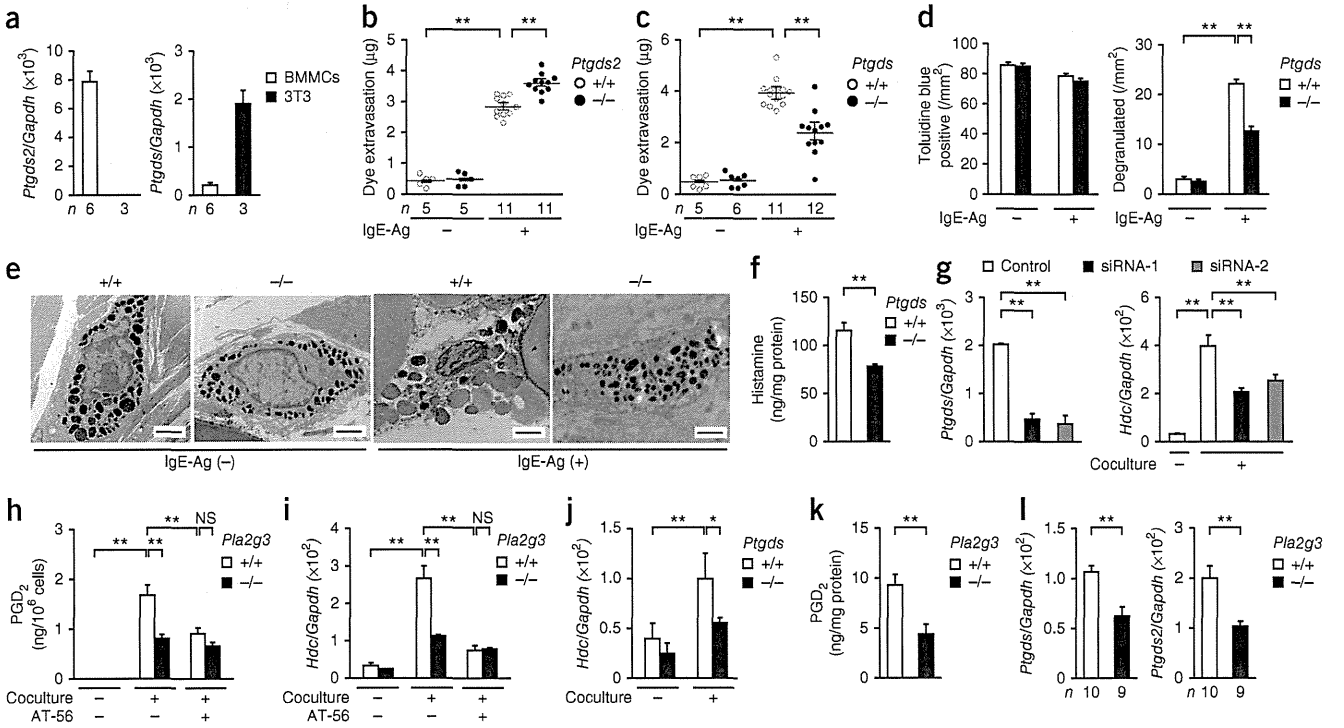

Figure 6 Defective mast-cell maturation and anaphylaxis by L-PGDS deficiency. (**a**) Expression of *Ptgds* and *Ptgds2* relative to *Gapdh* in wild-type BMMCs and Swiss 3T3 fibroblasts. (**b**,**c**) Quantification of ear edema in PCA in $Ptgds^{-/-}$ (**b**), $Ptgds2^{-/-}$ (**c**) mice (–/–) and littermate wild-type (+/+) mice with (IgE-Ag (+)) or without (IgE-Ag (–)) antigen challenge. (**d**) Dermal mast-cell counts in $Ptgds^{+/+}$ and $Ptgds^{-/-}$ mice before and 2 min after IgE-Ag–mediated PCA ($n = 6$). Number of degranulated mast cells were evaluated by staining of skin sections with toluidine blue, as in **Figure 2g**. (**e**) Transmission electron microscopy of $Ptgds^{+/+}$ (+/+) and $Ptgds^{-/-}$ (–/–) ear mast cells before (IgE-Ag (–)) and 2 min after (IgE-Ag (+)) antigen challenge. Scale bars, 2 μm. (**f**) Histamine levels in ears of $Ptgds^{+/+}$ and $Ptgds^{-/-}$ mice ($n = 10$). (**g**) *Ptgds* expression in Swiss 3T3 fibroblasts after *Ptgds* or scrambled siRNA treatment and *Hdc* expression in wild-type BMMCs before and on day 2 of coculture with siRNA-treated fibroblasts ($n = 7$). (**h**,**i**) PGD_2 generation (**h**) and *Hdc* expression (**i**) before and on day 1 of coculture of $Pla2g3^{+/+}$ or $Pla2g3^{-/-}$ BMMCs with Swiss 3T3 fibroblasts with or without AT-56 ($n = 6$). (**j**) *Hdc* expression in wild-type BMMCs before and on day 4 of coculture with $Ptgds^{+/+}$ (+/+) or $Ptgds^{-/-}$ (–/–) skin fibroblasts ($n = 6$). (**k**,**l**) PGD_2 levels ($n = 10$; **k**) and *Ptgds* and *Ptgds2* expression (**l**) in the ear skin of $Pla2g3^{+/+}$ and $Pla2g3^{-/-}$ mice. Data are compiled from two (**a**,**d**,**f**,**h**–**l**) or three (**b**,**c**,**g**) experiments (mean ± s.e.m., $*P < 0.05$; $**P < 0.01$; NS, not significant). Images in **e** are representative of two experiments.

regulatory pathway driving maturation of mast cells. The transfer of $Ptgds^{+/+}$ or $Ptgds^{-/-}$ BMMCs into $Kit^{W\text{-}sh/W\text{-}sh}$ mice fully restored the PCA response (**Supplementary Fig. 7b**), and a similar induction of *Hdc* occurred when $Ptgds^{+/+}$ or $Ptgds^{-/-}$ BMMCs were cultured with fibroblasts (**Supplementary Fig. 7c**), indicating that L-PGDS in fibroblasts, not in mast cells, may be important for the regulation of mast cells.

Coculture with L-PGDS–silenced Swiss 3T3 fibroblasts by two distinct *Ptgds*-specific small interfering (si)RNAs resulted in less induction of *Hdc* in wild-type CTMC-like cells (**Fig. 6g**). PGD_2 generation after coculture of parent fibroblasts with $Pla2g3^{-/-}$ BMMCs was ~50% lower than with $Pla2g3^{+/+}$ BMMCs (**Fig. 6h**). The L-PGDS inhibitor AT-56 lowered PGD_2 generation and *Hdc* induction in $Pla2g3^{+/+}$ cocultures to amounts similar to those in $Pla2g3^{-/-}$ cocultures, although it did not affect these responses in $Pla2g3^{-/-}$ cocultures (**Fig. 6h**,**i** and **Supplementary Fig. 7d**). *Hdc* induction in wild-type BMMCs also occurred in coculture with primary skin fibroblasts from $Ptgds^{+/+}$ mice, whereas this response was impaired in coculture with those from $Ptgds^{-/-}$ mice (**Fig. 6j**). Thus, the augmentative effects of PLA2G3 on coculture-driven synthesis of PGD_2 and histamine were abrogated when L-PGDS in fibroblasts was ablated. L-PGDS–dependent production of PGD_2, as revealed by coculture of $Ptgds2^{-/-}$ BMMCs with Swiss 3T3 fibroblasts, occurred gradually over a long period, whereas H-PGDS–dependent production of PGD_2 was transient, albeit robust (**Supplementary Fig. 7e**), suggesting that the continuous supply of PGD_2 by L-PGDS is crucial for maturation of mast cells.

Additionally, we observed robust upregulation of *Ptgds2* in BMMCs and *Ptgds* in Swiss 3T3 fibroblasts or in primary mouse skin fibroblasts (and to a much lesser extent in BMMCs) in wild-type BMMC cocultures, whereas these responses occurred only partially in $Pla2g3^{-/-}$ BMMC cocultures (**Supplementary Fig. 7f–h**). Conversely, induction of *Ptgds* in Swiss 3T3 fibroblasts was enhanced in coculture with $PLA2G3^{tg/+}$ BMMCs relative to wild-type BMMCs (**Supplementary Fig. 7i**). Thus, not only did mast cell–derived PLA2G3 supply arachidonic acid to L-PGDS in fibroblasts, it also contributed to induced expression of L-PGDS for efficient biosynthesis of a pool of PGD_2 that promotes maturation of mast cells. However, addition of PLA2G3 or BV-PLA_2 alone did not increase *Ptgds* expression in fibroblasts (**Supplementary Fig. 7j**), suggesting that some additional mast cell–derived factor(s) may be required for the induction of L-PGDS in fibroblasts. In agreement with the *in vitro* studies, amounts of PGD_2 (**Fig. 6k**) and expression of two PGDSs (**Fig. 6l**) were significantly lower in the ear of $Pla2g3^{-/-}$ mice than that of $Pla2g3^{+/+}$ mice, confirming the coupling of PLA2G3 with PGD_2 synthesis *in vivo*. Thus, PLA2G3 secreted from mast cells is

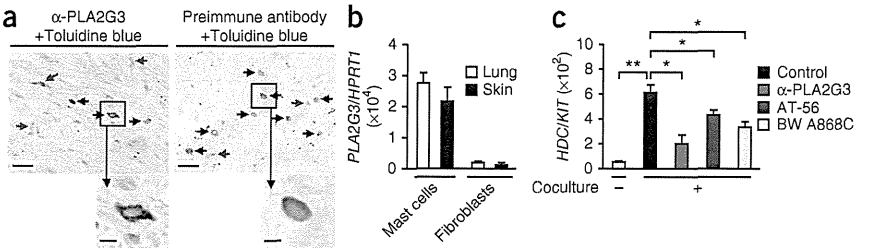

Figure 7 The PLA2G3–L-PGDS–DP1 axis facilitates maturation of human mast cells. (**a**) Immunohistochemistry analysis of human skin sections (atopic dermatitis) with anti-PLA2G3 (α-PLA2G3) or a preimmune antibody, followed by counterstaining with toluidine blue (scale bars, 50 μm). Blue and red arrows indicate resting and degranulated mast cells, respectively. Boxed areas are magnified below (scale bars, 5 μm). (**b**) Expression of *PLA2G3* relative to *HRPT1* in primary mast cells and fibroblasts obtained from human skin and lung ($n = 3$). (**c**) Expression of *HDC* relative to *KIT* in human lung mast cells before or on day 4 of coculture with human lung fibroblasts in the presence or absence of 5 μg/ml anti-PLA2G3, 10 μM AT-56 or 1 μM BW A868C ($n = 4$). Data are from one experiment (**b**,**c**; mean ± s.e.m., $*P < 0.05$; $**P < 0.01$). Images in **a** are representative of two experiments.

linked to fibroblastic L-PGDS–dependent synthesis of PGD_2, which in turn activates DP1 induced on mast cells to assist their terminal maturation toward a fully anaphylaxis-sensitive CTMC-like phenotype (**Supplementary Fig. 7k**).

PLA2G3 PGD_2 axis induces maturation of human mast cells

In human skin, toluidine blue$^+$ dermal mast cells showed PLA2G3 immunoreactivity, although some toluidine blue$^-$ cells also appeared PLA2G3$^+$ (**Fig. 7a**). We detected *PLA2G3* mRNA expression in mast cells in preference to fibroblasts obtained from human lung and skin (**Fig. 7b**). *HDC* mRNA expression was robustly induced in human lung mast cells after coculture with human lung fibroblasts, and this induction was suppressed either by anti-PLA2G3, by L-PGDS inhibitor (AT-56) or by DP1 antagonist (BW A868C) to a similar extent (**Fig. 7c**). Thus, the fibroblast-dependent *HDC* induction in human mast cells also depends on the PLA2G3–L-PGDS–DP1 pathway.

DISCUSSION

Here we showed that PLA2G3, a major $sPLA_2$ in mast cells, contributed to anaphylaxis by inducing maturation of mast cells in concert with adjacent fibroblasts through a unique pathway involving a cell-to-cell loop of the biosynthetic and receptor pathway for PGD_2. Promotion of mast cell maturation by PGD_2-DP1 signaling provides a mechanistic explanation for the protective effect of systemic DP1 ablation on asthma[9]. The paracrine PGD_2 circuit driven by PLA2G3, an 'anaphylactic $sPLA_2$', is a previously unidentified lipid-orchestrated pathway linked to allergy and uncovers a missing microenvironmental cue underlying the proper maturation of mast cells.

The SCF–c-Kit system, in cooperation with transcription factors, integrins or accessory cytokines, is essential for the development, homing, proliferation and differentiation of mast cells[3–7]. However, SCF alone is insufficient to drive the full maturation of mast cells, leading to the hypothesis that some other stromal factor(s) may be additionally required. These signals may include, for instance, interleukin 33, nerve growth factor, the morphogen TGF-β, hyaluronic acid and the adhesion molecule SgIGSF (spermatogenic immunoglobulin superfamily)[3,4,7], although their *in vivo* relevancies have not yet been fully understood. As in mice lacking PLA2G3, mast cells in mice lacking histamine (*Hdc*$^{-/-}$) or heparin (*Ndst2*$^{-/-}$ or *Srgn*$^{-/-}$) are immature and have low histamine content[32–34], suggesting that the lower amount of histamine may underlie, at least in part, the defective maturation of mast cells. We showed here that a signal driven by PGD_2, a bioactive lipid, is a missing link required for the fibroblast-driven maturation of mast cells. The PLA2G3–L-PGDS–DP1 circuit revealed the paracrine action of $sPLA_2$ in the biosynthetic mobilization of PGD_2 by proximal cells, the functional segregation of the two PGDS enzymes in distinct cell populations and a new aspect of PGD_2-DP1 signaling in promoting maturation of mast cells and thereby allergy. Moreover, our results revealed a previously unidentified aspect of the stromal cytokine SCF, which triggers this unique lipid-driven pathway by inducing PLA2G3 secretion from mast cells.

L-PGDS, a fibroblast-cell enzyme, acts downstream of PLA2G3 to supply PGD_2 to DP1 in mast cells to drive their terminal maturation. Contrary to our prediction, PGD_2 driven by H-PGDS, a mast cell enzyme, had an anti-allergy role, a view that is consistent with the exacerbated allergen-induced contact dermatitis in *Ptgds2*$^{-/-}$ mice[11]. Although it is unclear how the L-PGDS–driven extrinsic, but not the H-PGDS–driven intrinsic, pool of PGD_2 is preferentially used by DP1 on mast cells, we speculate that the prolonged supply of PGD_2 by L-PGDS, rather than its transient supply by H-PGDS, may be suitable for a long-lasting cell differentiation process. Alternatively, the PGD_2 captured by L-PGDS, a lipid carrier protein (lipocalin), may be stabilized or better presented to mast cell DP1. This idea is reminiscent of a finding that lysophosphatidic acid (LPA), another lipid mediator, is presented to its cognate receptor as a complex with autotaxin, an LPA-producing enzyme[35]. The spatiotemporal discrimination of distinct PGD_2 pools is also supported by the fact that although PGD_2 promotes Th2-based asthma[9], it contributes to resolution of inflammation through limiting neutrophil infiltration, dendritic cell activation or other mechanisms[11–13].

The paracrine PLA2G3–L-PGDS–DP1 circuit could not be compensated by other PLA_2 enzymes, implying a specific role of this atypical $sPLA_2$. We observed no defects in maturation of mast cells or anaphylaxis even in mice lacking $cPLA_2\alpha$, although mild developmental changes in *Pla2g4a*$^{-/-}$ BMMCs have been reported, probably because of different culture conditions[29]. Presumably, ablation of only the specific and local lipid mediator pathway by PLA2G3 deficiency, in contrast to ablation of bulk eicosanoids in both mast cells and microenvironments by $cPLA_2\alpha$ deficiency[29], may have a different impact on mast cells. The phenotypes observed in *Pla2g3*$^{-/-}$ mice tend to be more severe than those observed in *Ptgdr*$^{-/-}$ or *Ptgds*$^{-/-}$ mice, suggesting that PLA2G3 might be also coupled with other lipid signal(s) that could act in concert with the L-PGDS–DP1 axis to promote full maturation of mast cells. Such lipid candidates include LPA and lysophosphatidylserine, which can affect mast cell development and activation[36,37]. Not only can lysophospholipids transmit signals through their specific receptors, but they can also facilitate the opening of Ca^{2+} channels, which might explain the degranulation-promoting effect of PLA2G3 on mast cells.

Although it has been proposed that $sPLA_2$ enzymes, after being secreted, may act on neighboring cells or extracellular phospholipids to augment lipid mediator biosynthesis, this idea has yet to gain traction because *in vivo* evidence is largely lacking. Our study provides to our knowledge the first clear *in vivo* evidence that $sPLA_2$ acts in this

manner, thus providing a rationale for the long-standing question on the role of the secreted type of PLA_2. This extracellular PLA_2 family, through a paracrine process, regulates homeostasis and pathology in response to a given microenvironmental cue. Given that PLA2G3 is insensitive to classical $sPLA_2$ inhibitors, a new agent that specifically inhibits this unique $sPLA_2$ may be useful for the treatment of patients with mast cell–associated allergic and other diseases.

METHODS

Methods and any associated references are available in the online version of the paper.

Accession code. Gene Expression Ominibus: GSE44980 (microarray data).

Note: Supplementary information is available in the online version of the paper.

ACKNOWLEDGMENTS

We thank Y. Tanoue, H. Ohkubo, K. Araki and K. Yamamura for generating *Ptges2*$^{-/-}$ mice. This work was supported by grants-in-aid for Scientific Research from the Ministry of Education, Culture, Sports, Science and Technology of Japan (22116005 and 24390021 to M.M. and 23790119 and 24117724 to Y.T.), Promoting Individual Research to Nurture the Seeds of Future Innovation and Organizing Unique Innovative Network (PRESTO) of Japan Science and Technology Agency (to M.M.), and the Uehara, Mitsubishi, Terumo, Mochida and Toray Science Foundations (to M.M.).

AUTHOR CONTRIBUTIONS

Y.T. performed experiments and together with M.M. conceived and designed the study, interpreted the findings and wrote the manuscript; N.U., T.K., M.K., R.M. and H.S. performed experiments; S.T., M.S., Masanori Nakamura, Y.N., K.I., K.M., Satoshi Nakamizo, K.K., Y.O. and C.R. helped perform some experiments; K.Y., N.K., R.T., M.H.G. M.A., T.Y., Masataka Nakamura, K.W., H.H., Motonao Nakamura, K.A., Y.U., Y.S., T.S., Shu Narumiya and S.H. contributed to experimental designs.

COMPETING FINANCIAL INTERESTS

The authors declare no competing financial interests.

1. Galli, S.J. & Tsai, M. IgE and mast cells in allergic disease. *Nat. Med.* **18**, 693–704 (2012).
2. Gurish, M.F. & Austen, K.F. Developmental origin and functional specialization of mast cell subsets. *Immunity* **37**, 25–33 (2012).
3. Allakhverdi, Z., Smith, D.E., Comeau, M.R. & Delespesse, G. Cutting edge: The ST2 ligand IL-33 potently activates and drives maturation of human mast cells. *J. Immunol.* **179**, 2051–2054 (2007).
4. Matsuda, H. *et al.* Nerve growth factor induces development of connective tissue-type mast cells *in vitro* from murine bone marrow cells. *J. Exp. Med.* **174**, 7–14 (1991).
5. Abonia, J.P. *et al.* Constitutive homing of mast cell progenitors to the intestine depends on autologous expression of the chemokine receptor CXCR2. *Blood* **105**, 4308–4313 (2005).
6. Gurish, M.F. *et al.* Intestinal mast cell progenitors require CD49dβ7 (α4β7 integrin) for tissue-specific homing. *J. Exp. Med.* **194**, 1243–1252 (2001).
7. Ito, A. *et al.* SgIGSF: a new mast-cell adhesion molecule used for attachment to fibroblasts and transcriptionally regulated by MITF. *Blood* **101**, 2601–2608 (2003).
8. Shimizu, T. Lipid mediators in health and disease: enzymes and receptors as therapeutic targets for the regulation of immunity and inflammation. *Annu. Rev. Pharmacol. Toxicol.* **49**, 123–150 (2009).
9. Matsuoka, T. *et al.* Prostaglandin D_2 as a mediator of allergic asthma. *Science* **287**, 2013–2017 (2000).
10. Kanaoka, Y., Maekawa, A., Penrose, J.F., Austen, K.F. & Lam, B.K. Attenuated zymosan-induced peritoneal vascular permeability and IgE-dependent passive cutaneous anaphylaxis in mice lacking leukotriene C_4 synthase. *J. Biol. Chem.* **276**, 22608–22613 (2001).
11. Trivedi, S.G. *et al.* Essential role for hematopoietic prostaglandin D_2 synthase in the control of delayed type hypersensitivity. *Proc. Natl. Acad. Sci. USA* **103**, 5179–5184 (2006).
12. Hammad, H. *et al.* Activation of the D prostanoid 1 receptor suppresses asthma by modulation of lung dendritic cell function and induction of regulatory T cells. *J. Exp. Med.* **204**, 357–367 (2007).
13. Levy, B.D., Clish, C.B., Schmidt, B., Gronert, K. & Serhan, C.N. Lipid mediator class switching during acute inflammation: signals in resolution. *Nat. Immunol.* **2**, 612–619 (2001).
14. Kunikata, T. *et al.* Suppression of allergic inflammation by the prostaglandin E receptor subtype EP3. *Nat. Immunol.* **6**, 524–531 (2005).
15. Serhan, C.N., Chiang, N. & Van Dyke, T.E. Resolving inflammation: dual anti-inflammatory and pro-resolution lipid mediators. *Nat. Rev. Immunol.* **8**, 349–361 (2008).
16. Murakami, M. *et al.* Recent progress in phospholipase A_2 research: From cells to animals to humans. *Prog. Lipid Res.* **50**, 152–192 (2011).
17. Uozumi, N. *et al.* Role of cytosolic phospholipase A_2 in allergic response and parturition. *Nature* **390**, 618–622 (1997).
18. Munoz, N.M. *et al.* Deletion of secretory group V phospholipase A_2 attenuates cell migration and airway hyperresponsiveness in immunosensitized mice. *J. Immunol.* **179**, 4800–4807 (2007).
19. Henderson, W.R. Jr. *et al.* Importance of group X-secreted phospholipase A_2 in allergen-induced airway inflammation and remodeling in a mouse asthma model. *J. Exp. Med.* **204**, 865–877 (2007).
20. Bilo, B.M., Rueff, F., Mosbech, H., Bonifazi, F. & Oude-Elberink, J.N. Diagnosis of Hymenoptera venom allergy. *Allergy* **60**, 1339–1349 (2005).
21. Dudler, T. *et al.* A link between catalytic activity, IgE-independent mast cell activation, and allergenicity of bee venom phospholipase A_2. *J. Immunol.* **155**, 2605–2613 (1995).
22. Sato, H. *et al.* Group III secreted phospholipase A_2 regulates epididymal sperm maturation and fertility in mice. *J. Clin. Invest.* **120**, 1400–1414 (2010).
23. Murakami, M. *et al.* Cellular distribution, post-translational modification, and tumorigenic potential of human group III secreted phospholipase A_2. *J. Biol. Chem.* **280**, 24987–24998 (2005).
24. Murakami, M. *et al.* Cellular arachidonate-releasing function of novel classes of secretory phospholipase A_2s (groups III and XII). *J. Biol. Chem.* **278**, 10657–10667 (2003).
25. Valentin, E., Ghomashchi, F., Gelb, M.H., Lazdunski, M. & Lambeau, G. Novel human secreted phospholipase A_2 with homology to the group III bee venom enzyme. *J. Biol. Chem.* **275**, 7492–7496 (2000).
26. Sato, H. *et al.* Analyses of group III secreted phospholipase A_2 transgenic mice reveal potential participation of this enzyme in plasma lipoprotein modification, macrophage foam cell formation, and atherosclerosis. *J. Biol. Chem.* **283**, 33483–33497 (2008).
27. Taketomi, Y. *et al.* Impaired mast cell maturation and degranulation and attenuated allergic responses in *Ndrg1*-deficient mice. *J. Immunol.* **178**, 7042–7053 (2007).
28. Kashem, S.W. *et al.* G protein coupled receptor specificity for C3a and compound 48/80-induced degranulation in human mast cells: roles of Mas-related genes MrgX1 and MrgX2. *Eur. J. Pharmacol.* **668**, 299–304 (2011).
29. Nakatani, N. *et al.* Role of cytosolic phospholipase A_2 in the production of lipid mediators and histamine release in mouse bone-marrow-derived mast cells. *Biochem. J.* **352**, 311–317 (2000).
30. Mohri, I. *et al.* Prostaglandin D_2-mediated microglia/astrocyte interaction enhances astrogliosis and demyelination in twitcher. *J. Neurosci.* **26**, 4383–4393 (2006).
31. Eguchi, N. *et al.* Lack of tactile pain (allodynia) in lipocalin-type prostaglandin D synthase-deficient mice. *Proc. Natl. Acad. Sci. USA* **96**, 726–730 (1999).
32. Ohtsu, H. *et al.* Mice lacking histidine decarboxylase exhibit abnormal mast cells. *FEBS Lett.* **502**, 53–56 (2001).
33. Forsberg, E. *et al.* Abnormal mast cells in mice deficient in a heparin-synthesizing enzyme. *Nature* **400**, 773–776 (1999).
34. Humphries, D.E. *et al.* Heparin is essential for the storage of specific granule proteases in mast cells. *Nature* **400**, 769–772 (1999).
35. Nishimasu, H. *et al.* Crystal structure of autotaxin and insight into GPCR activation by lipid mediators. *Nat. Struct. Mol. Biol.* **18**, 205–212 (2011).
36. Bagga, S. *et al.* Lysophosphatidic acid accelerates the development of human mast cells. *Blood* **104**, 4080–4087 (2004).
37. Iwashita, M. *et al.* Synthesis and evaluation of lysophosphatidylserine analogues as inducers of mast cell degranulation. Potent activities of lysophosphatidylthreonine and its 2-deoxy derivative. *J. Med. Chem.* **52**, 5837–5863 (2009).

ONLINE METHODS

Mice. *Pla2g3*$^{-/-}$, *Pla2g4a*$^{-/-}$, *Pla2g5*$^{-/-}$, *Pla2g10*$^{-/-}$, *Ptgdr*$^{-/-}$, *Ptgdr2*$^{-/-}$, *Ptgds*$^{-/-}$, *Ptgds2*$^{-/-}$, *Ptges*$^{-/-}$, *Ptger1*$^{-/-}$, *Ptger2*$^{-/-}$, *Ptger3*$^{-/-}$, *Ptger4*$^{-/-}$, *Ptgfr*$^{-/-}$, *Ptgir*$^{-/-}$, *Tbxa2r*$^{-/-}$, *Ltb4r1*$^{-/-}$, *Ltb4r2*$^{-/-}$, *Ltc4s*$^{-/-}$, *Alox15*$^{-/-}$ and *PLA2G3*$^{tg/+}$ mice have been described previously[9,14,17–19,22,26,38–44]. *Ptges2*$^{-/-}$ mice (RIKEN RBRC04849) were generated by the Institute of Resource Development and Analysis (Kumamoto University). *Pla2g2d*$^{-/-}$, *Pla2g2e*$^{-/-}$ and *Pla2g2f*$^{-/-}$ mice were generated by the Transgenic Resources Program (Department of Comparative Medicine, University of Washington; unpublished data). These mice were backcrossed to C57BL/6 mice for more than 11 generations, except for *Pla2g3*$^{-/-}$ and *Ptger4*$^{-/-}$ mice (129Sv × C57BL/6), which were from the third backcrosses to C57BL/6 mice owing to severe problems in reproduction[22] and neonatal death[39], respectively, particularly after successive backcrossing onto the C57BL/6 background. All experiments using knockout or transgenic mice (male, 8–12-week-old) were compared with their age-matched littermate control mice. Mast cell–deficient *Kit* mutant mice, C57BL/6J-*Kit*$^{W-sh/W-sh}$ and WBB6F$_1$-*Kit*$^{W/W-v}$, were purchased from the Jackson Laboratories and Japan SLC, respectively. All mice were housed in climate-controlled (23 °C) specific pathogen–free facilities with a 12-h light-dark cycle, with free access to standard laboratory food (CE2; CLEA) and water. All animal experiments were performed in accordance with protocols approved by the Institutional Animal Care and Use Committees of the Tokyo Metropolitan Institute of Medical Science and Showa University, in accordance with the Standards Relating to the Care and Management of Experimental Animals in Japan.

PLA$_2$ assay. BV-PLA$_2$ was purchased from Sigma-Aldrich. Recombinant mature human PLA2G3 protein was expressed in silkworms by the baculovirus system and purified to near homogenity by an affinity column conjugated with mouse monoclonal anti–human PLA2G3 (5D2F1; IgG), as described previously[26]. PLA$_2$ activities in the supernatants of mast cells were assayed by measuring the amounts of [^{14}C]linoleic acid released from 1-palmitoyl-2-[^{14}C]linoleoyl-phosphatidylethanolamine (Perkin Elmer). Each reaction mixture consisted of appropriate amounts of the samples, 100 mM Tris-HCl (pH 7.4), 4 mM $CaCl_2$ and the substrate at 1 μM. After incubation for 2 h at 37 °C, [^{14}C]linoleic acid was extracted, and the radioactivity was quantified with a liquid scintillation counter (LS5801; Beckman), as described previously[22–24].

Anaphylaxis. For PSA, mice were intravenously injected with 3 μg of monoclonal anti-DNP IgE (SPE-7; Sigma-Aldrich). After 24 h, the mice were challenged intravenously with 25 or 500 μg of DNP-conjugated human serum albumin (HSA; Sigma-Aldrich)[27]. Then, the rectal temperature was measured for 120 min with an electronic thermometer (Physitemp Instruments). For PCA, mice were passively sensitized by intradermal injection with 30 ng of anti-DNP IgE. After 24 h, the mice were challenged by intravenous injection of 20 or 60 μg of DNP-HSA in saline containing Evans blue dye (Wako)[27]. Extravasation of blue dye in the ear was monitored for 30 min, and ear biopsies were incubated at 37 °C in 3 N KOH. Quantitative analysis of the extracts was performed by measuring the absorbance of blue dye at 620 nm. For active anaphylaxis, mice were immunized intraperitoneally on days 0 (day when OVA was first administered), 7 and 14 with 10 μg of chicken OVA (Sigma-Aldrich) in 100 μl of saline mixed with 200 μl of alum (Alu Gel S, which contained 2% $Al(OH)_3$; Serva). Seven days after the last immunization, the left and right ears of mice were injected intradermally with 30 μg of OVA. Net ear swelling was measured at 30 min after challenge with OVA.

Measurement of histamine and protease activities. The procedures were described previously[27]. Briefly, tissues were homogenized in PBS with a bead crusher (μT-01; Taitec) at 4 °C, and Triton X-100 was added to a final concentration of 0.5% (v/v). For the histamine assay, the lysates were treated with 3% (v/v) perchloric acid and left for 30 min on ice, and the resulting supernatants (tissue extracts) after centifugation at 10,000*g* for 30 min at 4 °C were applied to a cation-exchange WCX-1 column on HPLC (Shimadzu) to separate histamine, which was then measured fluorometrically by the *o*-phthalaldehyde method[45]. For the protease assay, 10 μl of the tissue extracts were diluted with 90 μl of 50 mM Tris-HCl (pH 8.3), followed by incubation with 20 μl of 1.8 mM chromogenic substrates for chymotrypsin- or trypsin-like proteases (S-2586 and S-2288, respectively; Chromogenix) and CPA (M-2245; Bachem) at 37 °C for 1–3 min. Changes in absorbance at 405 nm were measured.

Culture of mouse BMMCs and other bone marrow–derived cells. To prepare BMMCs, mouse bone marrow (BM) cells were cultured in IL-3–containing BMMC complete medium[27]. After 4–6 weeks of culture, >97% of the cells were identified as Kit$^+$FcεRIα$^+$ mast cells by flow cytometry. The coculture-driven maturation of immature BMMCs toward CTMC-like cells has been described previously[27]. Briefly, BMMCs were seeded onto Swiss 3T3 fibroblast monolayer and cocultured for the appropriate durations (typically for 4 d) in the presence of mouse SCF (100 ng/ml; Peprotech). The cells were trypsinized and reseeded in culture dishes, and nonadherent cells were collected. Purity (>99%) was confirmed by flow cytometry for Kit and FcεRIα. Maturation of BMMCs into CTMC-like cells was verified by staining their granules with alcian blue and counterstaining with safranin O. As required for experiments, 10 μM AT-56, 1 μM BW A868C, 10 μM BW 245C (Cayman Chemical) or 10 μM forskolin (Sigma-Aldrich) were added to the coculture.

BM cells were cultured with mouse granulocyte-macrophage colony stimulating factor (GM-CSF; 10 ng/ml; Peprotech) for 9 d, mouse macrophage colony stimulating factor (M-CSF; 100 ng/ml; Kyowa Kirin) for 3 d or mouse TSLP (1 μg/ml; R&D Systems) for 5 d in RPMI1640 medium (Invitrogen) containing 10% (v/v) FBS (Invitrogen) to obtain BMDCs, BMDMs or BM basophils, respectively[46,47]. The purity of each cell population was verified by flow cytometry for the expression of CD11c and MHC class II for BMDCs, the expression of F4/80 and CD11b for BMDMs, and the expression of FcεRIα and CD200R3 (or DX5α) coupled with a lack of expression of Kit for BM basophils (see below).

Activation of BMMCs. BMMCs (10^6 cells) before and after coculture with fibroblasts were sensitized with 1 μg/ml anti-DNP IgE for 2 h and then stimulated with various concentrations (typically 100 ng/ml) of DNP-BSA (Sigma-Aldrich), 100 ng/ml mouse SCF or 10 μg/ml C48/80 (Sigma-Aldrich). Degranulation was evaluated by measuring histamine or β-HEX release, as described previously[27]. The levels of eicosanoids were determined by ELISA in accordance with the manufacturer's instructions (Cayman Chemical). Expression of cytokines was assessed by real-time PCR. Lactate dehydrogenase activity was measured using an LDH Cytotoxicity Detection Kit (Takara).

Preparation and activation of mouse pMCs. To collect peritoneal cells, 5 ml of Hank's balanced salt solution (Invitrogen) was injected into the mouse peritoneal cavity, and the abdomen was massaged gently. After collecting peritoneal cells from the peritoneal fluid, they were resuspended in PIPES-buffered saline for electron microscopy or in BMMC-complete medium for degranulation assay. For degranulation, 10^6 cells were treated for 30 min with 1–5 μg/ml of human PLA2G3 or BV-PLA$_2$, with 1 μM A23187 (Sigma-Aldrich), or with 1 μg/ml anti-DNP IgE for 1 h and then with 100 ng/ml DNP-BSA for 30 min in the presence of 4 μM lysophosphatidylserine (Avanti Polar Lipids). The release of histamine was then evaluated.

Preparation of mouse skin mast cells and fibroblasts. Mouse ear skin was dispersed with 1.6 mg/ml collagenase type II (Worthington) and 0.1 mg/ml DNase I (Sigma-Aldrich) in RPMI1640 containing 10% FBS for 30 min at 37 °C and passed through a cell strainer (40-μm mesh size). Skin mast cells were identified as Kit$^+$FcεRIα$^+$ cells after CD45 gating by flow cytometry. The skin-dispersed cells were cultured in RPMI1640 containing 10% FBS, trypsinized and reseeded on culture dishes, and adherent cells grown to confluency were used as skin fibroblasts.

Preparation and culture of human mast cells and fibroblasts. Preparation and culture of mast cells from human skin and lung were performed as described previously[48]. Briefly, macroscopically normal human lung or skin tissue was obtained during surgery at the Nihon University Hospital under approval of the faculty ethics committee and informed consent from the patient. Lung and skin cells were dispersed from chopped lung and foreskin specimens by collagenase and hyaluronidase (Sigma-Aldrich). These cells were maintained for 6 weeks in MethoCult SF^{BIT} (Iscove's modified Dulbecco's medium (IMDM)-based serum-free medium containing 1.2% (w/v) methylcellulose;

doi:10.1038/ni.2586

Veritas) supplemented with human SCF (100 ng/ml; Peprotech) and human IL-6 (50 ng/ml; Peprotech). On day 42, methylcellulose was dissolved in PBS, and the cells were resuspended and cultured in IMDM medium (Invitrogen) containing 0.1% BSA, 100 ng/ml SCF and 50 ng/ml IL-6. The purity of human mast cells, as assessed with metachromatic staining, was more than 97%. Human skin and lung fibroblasts (CC-2511 and CC-2512, respectively) and their culture medium were purchased from Lonza. Human lung mast cells (5×10^5 cells) were seeded onto the human lung fibroblast monolayer and cocultured for 4 d in 500 µl of IMDM medium plus 2% FBS in the presence of SCF and IL-6, with medium change at 2-d intervals. The cells were trypsinized and reseeded in culture dishes, and nonadherent cells were collected. The purity of mast cells was normalized based on the expression of *KIT*.

Real-time PCR. Total RNA was extracted from tissues and cells using TRIzol reagent (Invitrogen). First-strand cDNA synthesis was performed using the High-Capacity cDNA Reverse-Transcriptase Kit (Applied Biosystems). PCRs were carried out using the TaqMan Gene Expression System (Applied Biosystems) on an ABI7700 Real-Time PCR system (Applied Biosystems). The probe-primer sets are listed in **Supplementary Table 2**.

Measurement of intracellular Ca^{2+} levels. Intracellular Ca^{2+} levels were measured as described previously[27]. Briefly, IgE-sensitized BMMCs on coverslips were loaded for 60 min with the fluorescent Ca^{2+} indicator fura-2/AM (5 µM; Invitrogen) in Tyrode-HEPES buffer (pH 7.4) containing 2.5 mM probenecid, 0.04% (v/v) pluronic acid and 1% (v/v) serum. Then, the cells were washed and stimulated with antigen. Fura-2 fluorescence images were obtained using an image analyzer (ARGUS-50; Hamamatsu Photonics) with excitation at 340 nm (F340) and 380 nm (F380) at 5-s intervals. The fluorescence ratio (F340/F380) was calculated using US National Institutes of Health ImageJ software.

Western blotting. Tissue homogenates (20 µg protein equivalent) or BMMCs (2×10^5 cells) were lysed in SDS-PAGE sample buffer (63 mM Tris-HCl (pH 6.8), 2% (w/v) SDS, 10% (v/v) glycerol, and 0.08% (w/v) bromophenol blue) containing 5% (v/v) 2-mercaptoethanol, and then subjected to SDS-PAGE. Proteins were subsequently blotted onto PVDF membranes (Bio-Rad), followed by blocking with 5% (w/v) milk powder in PBS containing 0.05% (v/v) Tween 20 (PBS-T). The membranes were probed with rabbit polyclonal antibodies to HDC[49], H-PGDS[30], Kit (18101; IBL), PLCγ2 (3872; Cell Signaling), phospho-PLCγ2 Y1217 (3871; Cell Signaling), cPLA$_2$α (2832; Cell Signaling) or phospho-cPLA$_2$α S505 (2831; Cell Signaling) or mouse monoclonal antibodies against Akt (D9E; Cell Signaling), phospho-Akt S473 (C67E7; Cell Signaling), ERK1/2 (MK12; BD Transduction Laboratories), phospho-ERK1/2 T202/Y204 (20A; BD Transduction Laboratories), JNK (37; BD Transduction Laboratories), phospho-JNK T183/Y185 (41; BD Transduction Laboratories), p38 (27; BD Transduction Laboratories) or phospho-p38 MAPK T180/Y182 (30; BD Transduction Laboratories) at 1:500–1:2,000 dilutions in PBS-T containing 1% (w/v) milk powder or in Can Get Signal Solution 1 (Toyobo) for 1.5 h. After membranes were washed, the membranes were incubated for 1 h with horseradish peroxidase (HRP)-conjugated anti-rabbit (AP156P; Chemicon) or anti-mouse (21040; Molecular Probes) IgG at 1:5,000 dilution in PBS-T containing 1% milk powder or in Can Get Signal Solution 2 (Toyobo), and then visualized with ECL Prime western blotting detection reagent (GE Healthcare Life Science) on LAS-4000 (Fuji Film).

Histological analysis. Ears were fixed in 10% (v/v) neutral buffered formalin, embedded in paraffin and cut using a microtome. The sections (4 µm thickness) were stained with 0.05% toluidine blue (pH 0.5) for the detection of mast cells. Degranulated mast cells were defined as those showing the release of cellular granules. For immunohistochemistry, sections were incubated in PBS containing 5% normal goat serum, 5% BSA and 0.025% Triton X-100 for 20 min and then immunostained with a rabbit polyclonal to human PLA2G3, which reacts with both mature human and mouse enzymes (whose homology is 83%)[22–24], and mouse L-PGDS[50], at dilutions of 1:200 and 1:1,000, respectively, in the same buffer at 4 °C overnight. These preparations were incubated with biotinylated goat anti-rabbit IgG (BA-1000; Vector Laboratories) in PBS containing 5% BSA, 0.025% Triton X-100 and 10% mouse serum for 30 min followed by incubation with avidin DH and biotinylated HRP (Vectastain ABC kit; Vector Laboratories). These preparations were stained with 0.5 mg/ml 3,3′-diaminobenzidine and 0.1% (v/v) hydrogen peroxide solution. Human tissue sections were obtained from Chiba University following approval by the faculty ethical committee and informed consent from the patient. For transmission microscopy, tissues or cells were fixed with 0.1 M sodium cacodylate buffer (pH 7.2) containing 1% (v/v) glutaraldehyde and 4% (w/v) paraformaldehyde, post-fixed with 2% (w/v) OsO_4 in PBS, dehydrated by a graded ethanol series, passed through propylene oxide and embedded in Poly/Bed812 EPON (Polyscience). Ultrathin sections (0.08-µm thickness) were stained with uranyl acetate and lead citrate and then examined using an electron microscope (H-7600; Hitachi).

Adoptive transfer of BMMCs into mast cell–deficient mice. BMMCs obtained from 8–12-week-old male mice were reconstituted by intradermal (10^6 cells) or intravenous (10^7 cells) injection into 6-week-old male *Kit*$^{W\text{-}sh/W\text{-}sh}$ mice. Six weeks after intradermal transfer or 12 weeks after intravenous transfer of BMMCs, the mice were subjected to IgE-Ag–induced PCA, as described above. Alternatively, mast cells from the base to the tip of the ears from these mice were evaluated by toluidine blue staining or by real-time PCR of mast cell marker genes.

Flow cytometry. Cells were stained with either a labeled monoclonal antibody or an isotype-matched control antibody (hamster IgG (HTK888), mouse IgG_1 (MOPC-21), rat IgG_{2a} (RTK2758) or rat IgG_{2b} (RTK4530); BioLegend) and analyzed by flow cytometry using FACSCalibur (BD Biosciences) or FACSAria III Cell Sorter (BD Biosciences) with FlowJo software (Tree Star). The antibodies used were specific for mouse Kit (2B8; BD Biosciences), FcεRIα (MAR-1; eBioscience), DX5 (DX5; eBioscience), CD200R3 (Ba13; BioLegend), CD45 (30-F11; eBioscience), CD11c (N418; eBioscience), MHC class II (M5/114.15.2; eBioscience), CD11b (M1/70; BioLegend), F4/80 (BM8; BioLegend), CD45R/B220 (RA3-6B2; BD Biosciences), CD3ε (145–2X11; eBioscience), Gr-1 (RB-8C5; BioLegend), FOXP3 (150D; BioLegend) and FR4 (12A5; BioLegend).

Microarray. Total RNA was extracted from BMMCs derived from *Pla2g3*$^{-/-}$ and *Pla2g3*$^{+/+}$ mice before and after coculture and purified using the RNeasy Mini Kit (Qiagen). The quality of RNA was assessed with a 2100 Bioanalyzer (Agilent Technologies). Both cDNA and cRNA were synthesized with a Low Input Quick Amp Labeling Kit according to the manufacturer's protocol (Agilent Technologies). Samples were hybridized to the Whole Mouse Genome Microarray Kit (4 × 44K; Agilent Technologies), washed and then scanned using a Laser Scanner GenePix 4000B (Molecular Devices). Microarray data were analyzed with Feature Extraction software (Agilent Technologies) and then imported into GeneSpringGX11.5 (Agilent Technologies). Probes were normalized by quantile normalization among all microarray data.

RNA interference. Swiss 3T3 fibroblasts were cultured in 12-well plates to 50% confluence and transfected with a Mission predesigned siRNA construct (20 nM) for *Ptgds* (SASI_Mm01_00116073 or 00116081; Sigma-Aldrich) or a scrambled control siRNA (Invitrogen) using oligofectamine (Invitrogen), according to the manufacturer's instructions. After 48 h, wild-type BMMCs were cocultured for 2 d with the transfected cells.

Electrospray ionization mass spectrometry (ESI-MS). ESI-MS lipidomics analysis using a 4000Q TRAP quadrupole-linear ion trap hybrid mass spectrometer (AB SCIEX) with an UltiMate 3000 nano/cap/micro-liquid chromatography system (Dionex Corporation) combined with an HTS PAL autosampler (CTC Analytics AG) was performed as described previously[44]. Briefly, phospholipids extracted from 10^7 BMMCs were subjected directly to ESI-MS analysis by flow injection; typically, 3 µl (3 nmol phosphorous equivalent) of sample was applied. The mobile phase composition was acetonitrile/methanol/water (v/v/v = 6/7/2) plus 0.1% (v/v) ammonium formate (pH 6.8) at a flow rate of 10 µl/min. The scan range of the instrument was set at *m/z* 200–1,000 at a scan speed of 1,000 Da/s. The trap fill-time was set at 3 ms in the positive ion mode and at 5 ms in the negative ion mode. The ion spray voltage was set at 5,500 V in the positive ion mode and at −4,500 V in the negative ion

mode. Nitrogen was used as a curtain gas (at a setting of 10 arbitrary units) and as a collision gas (set to 'high').

Statistical analysis. The Excel Statistical Program File ystat 2008 (Igaku Tosho Shuppan) was used to determine statistical significance evaluated by an unpaired Student's *t*-test for two groups or an analysis of variance (ANOVA) for multiple groups. *P* values of less than 0.05 and 0.01 were considered statistically significant. Data are presented as the mean ± s.e.m.

38. Satoh, T. *et al.* Prostaglandin D_2 plays an essential role in chronic allergic inflammation of the skin via CRTH2 receptor. *J. Immunol.* **177**, 2621–2629 (2006).
39. Segi, E. *et al.* Patent ductus arteriosus and neonatal death in prostaglandin receptor EP4-deficient mice. *Biochem. Biophys. Res. Commun.* **246**, 7–12 (1998).
40. Sugimoto, Y. *et al.* Failure of parturition in mice lacking the prostaglandin F receptor. *Science* **277**, 681–683 (1997).
41. Kobayashi, T. *et al.* Roles of thromboxane A_2 and prostacyclin in the development of atherosclerosis in *apoE*-deficient mice. *J. Clin. Invest.* **114**, 784–794 (2004).
42. Iizuka, Y. *et al.* Protective role of the leukotriene B_4 receptor BLT2 in murine inflammatory colitis. *FASEB J.* **24**, 4678–4690 (2010).
43. Sun, D. & Funk, C.D. Disruption of 12/15-lipoxygenase expression in peritoneal macrophages. Enhanced utilization of the 5-lipoxygenase pathway and diminished oxidation of low density lipoprotein. *J. Biol. Chem.* **271**, 24055–24062 (1996).
44. Ueno, N. *et al.* Analysis of two major intracellular phospholipases A_2 (PLA_2) in mast cells reveals crucial contribution of cytosolic $PLA_2\alpha$, not Ca^{2+}-independent $PLA_2\beta$, to lipid mobilization in proximal mast cells and distal fibroblasts. *J. Biol. Chem.* **286**, 37249–37263 (2011).
45. Shore, P.A., Burkhalter, A. & Cohn, V.H. Jr. A method for the fluorometric assay of histamine in tissues. *J. Pharmacol. Exp. Ther.* **127**, 182–186 (1959).
46. Lutz, M.B. *et al.* An advanced culture method for generating large quantities of highly pure dendritic cells from mouse bone marrow. *J. Immunol. Methods* **223**, 77–92 (1999).
47. Siracusa, M.C. *et al.* TSLP promotes interleukin-3-independent basophil haematopoiesis and type 2 inflammation. *Nature* **477**, 229–233 (2011).
48. Kajiwara, N. *et al.* Activation of human mast cells through the platelet-activating factor receptor. *J. Allergy Clin. Immunol.* **125**, 1137–1145 (2010).
49. Tanaka, S. *et al.* Expression of l-histidine decarboxylase in granules of elicited mouse polymorphonuclear leukocytes. *Eur. J. Immunol.* **34**, 1472–1482 (2004).
50. Gerena, R.L., Eguchi, N., Urade, Y. & Killian, G.J. Stage and region-specific localization of lipocalin-type prostaglandin D synthase in the adult murine testis and epididymis. *J. Androl.* **21**, 848–854 (2000).

doi:10.1038/ni.2586

Anti-inflammatory role of PGD_2 in acute lung inflammation and therapeutic application of its signal enhancement

Takahisa Murata[a,1], Kosuke Aritake[b], Yoshiki Tsubosaka[a], Toshihiko Maruyama[b], Takayuki Nakagawa[c], Masatoshi Hori[a], Hiroyuki Hirai[d], Masataka Nakamura[e], Shuh Narumiya[f], Yoshihiro Urade[b], and Hiroshi Ozaki[a]

[a]Department of Veterinary Pharmacology, Graduate School of Agriculture and Life Sciences, University of Tokyo, Tokyo 113-8657, Japan; [b]Department of Molecular Behavioral Biology, Osaka Bioscience Institute, Osaka 565-0874, Japan; [c]Department of Veterinary Surgery, Graduate School of Agriculture and Life Sciences, University of Tokyo, Tokyo 113-8657, Japan; [d]Advanced Medicine and Development, BML, Inc., Saitama 350-1101, Japan; [e]Human Gene Sciences Center, Tokyo Medical and Dental University, Tokyo 113-8150, Japan; and [f]Department of Pharmacology, Faculty of Medicine, Kyoto University, Kyoto 606-8315, Japan

Edited by Charles N. Serhan, Brigham and Women's Hospital, Harvard Medical School, Boston, MA, and accepted by the Editorial Board February 15, 2013 (received for review October 17, 2012)

We investigated the role of prostaglandin D_2 (PGD_2) signaling in acute lung injury (ALI), focusing on its producer–effector interaction in vivo. Administration of endotoxin increased edema and neutrophil infiltration in the WT mouse lung. Gene disruption of hematopoietic PGD synthase (H-PGDS) aggravated all of the symptoms. Experiments involving bone marrow transplantation between WT and H-PGDS–deficient mice showed that PGD_2 derived from alveolar nonhematopoietic lineage cells (i.e., endothelial cells and epithelial cells) promotes vascular barrier function during the early phase (day 1), whereas neutrophil-derived PGD_2 attenuates its own infiltration and cytokine expression during the later phase (day 3) of ALI. Treatment with either an agonist to the PGD_2 receptor, DP, or a degradation product of PGD_2, 15-deoxy-$\Delta^{12,14}$-PGJ_2, exerted a therapeutic action against ALI. Data obtained from bone marrow transplantation between WT and DP-deficient mice suggest that the DP signal in alveolar endothelial cells is crucial for the anti-inflammatory reactions of PGD_2. In vitro, DP agonism directly enhanced endothelial barrier formation, and 15-deoxy-$\Delta^{12,14}$-PGJ_2 attenuated both neutrophil migration and cytokine expression. These observations indicate that the PGD_2 signaling between alveolar endothelial/epithelial cells and infiltrating neutrophils provides anti-inflammatory effects in ALI, and suggest the therapeutic potential of these signaling enhancements.

vascular permeability | pneumonia | lipid mediator | respiratory infection

Acute lung injury (ALI) and its severe manifestation, acute respiratory distress syndrome (ARDS), represent a clinical syndrome that results from multiple causes, including microbial infection and toxic inhalation. The most characteristic pathological findings of ALI/ARDS are neutrophil accumulation and alveolar edema caused by endothelial/epithelial barrier disruption (1). No specific pharmacologic therapies are currently available, and the mortality rate for ALI/ARDS remains very high (1). Thus, there is an urgent need to elucidate in detail the underlying pathogenesis of ALI/ARDS to develop new drugs against it.

Cyclooxygenase (COX), particularly COX-2 and its metabolites, the prostaglandins (PGs), play critical roles in the inflammatory response. Elevated PG levels have been reported in bronchoalveolar lavage (BAL) fluid obtained from patients with ARDS (2). In experimental models, Hinshaw et al. (3) originally found that COX inhibition prevents the development of sepsis and improves survival rates in dogs. Another group reported that COX-2 inhibition attenuated carrageenan-induced rat ALI (4). These findings suggest that COX-mediated production of PGs is crucial for the initiation and progression of lung inflammation. However, in a clinical study, treatment with the nonselective COX inhibitor ibuprofen did not reduce the incidence of ARDS in patients with sepsis (5). These observations suggest that PGs play a multifaceted role in the pathophysiology of airway inflammation, with both proinflammatory and anti-inflammatory components. The bioactions of each class of PGs are influenced by multiple causes. Types of PG-producing cells and their effector cells vary with both the causative pathogen and the stage of disease. The overall response of effector cells is determined by both receptors and cellular events. Thus, determining the precise contribution by an individual class of PGs regarding the functional partnership of its producer and effector cells at each disease stage is indispensable for future management of ALI/ARDS.

PGD_2 is one of the COX metabolites reported to mediate an inflammatory response (6). The hematopoietic-type PGD_2 synthase (H-PGDS) is expressed mainly in hematopoietic lineage cells, such as mast cells and Th2 cells. PGD_2 displays its bioactivity through the G protein-coupled receptor DP and/or the chemoattractant receptor-homologous molecule expressed on Th2 cells (CRTH2). Several previous studies have demonstrated that DP signal activation inhibits the migration and/or activation of eosinophils, basophils, dendritic cells, and Th2 cells (6). On the other hand, CRTH2 signal activation results in the migration of eosinophils and Th2 cells (7, 8). The dehydration product of PGD_2, 15-deoxy-$\Delta^{12,14}$-PGJ_2 (15d-PGJ_2), also modulates inflammatory responses via peroxisome proliferator-activated receptor (PPAR)-γ–dependent or –independent signal activation (9). Like the other PGs, PGD_2 presumably changes its pathophysiological contribution through these signal pathways depending on the target tissue, type of stimulus, and stage of the disease.

In a previous study, we focused on the physiological function of PGD_2-DP signaling in neovascular endothelial cells of tumors, and found that stimulation of this pathway enhanced endothelial barrier function and suppressed tumor angiogenesis (10). Given that vascular endothelial cells and alveolar epithelial cells form their respective barriers in the lung, which is a crucial determinant of lung inflammation, these observations led us to hypothesize that PGD_2 might play a protective role in ALI/ARDS. Consequently, in the present study we attempted to explore the pathophysiological implications of PGD_2 biosynthesis in the development ALI/ARDS

Author contributions: T. Murata and Y.U. designed research; T. Murata, K.A., Y.T., and T. Maruyama performed research; T. Murata, K.A., T.N., M.H., H.H., M.N., S.N., Y.U., and H.O. contributed new reagents/analytic tools; T. Murata, K.A., Y.T., and T. Maruyama analyzed data; and T. Murata wrote the paper.

The authors declare no conflict of interest.

This article is a PNAS Direct Submission. C.N.S. is a guest editor invited by the Editorial Board.

[1]To whom correspondence should be addressed. E-mail: amurata@mail.ecc.u-tokyo.ac.jp.

This article contains supporting information online at www.pnas.org/lookup/suppl/doi:10.1073/pnas.1218091110/-/DCSupplemental.

by focusing on the interaction between alveolar endothelial/epithelial cells and infiltrating neutrophils.

Results

Host H-PGDS Deficiency Accelerates Lung Inflammation. Under normal conditions, H-PGDS–deficient (H-PGDS$^{-/-}$) mice did not display any functional defect in respiratory gas exchange, as quantified by arterial partial pressure of oxygen (pO_2) values (Fig. 1*A*). Intratracheal administration of lipopolysaccharide (LPS), 3.75 mg/kg for 3 d, impaired respiratory function in both WT and H-PGDS$^{-/-}$ mice. Compared with the WT mice, the H-PGDS$^{-/-}$ mice exhibited more severe lung damage and a lower survival rate (Fig. 1*B*).

Morphological studies showed that the LPS challenge induced neutrophil infiltration in the lungs of WT mice by day 3 (Fig. 1*C*). The H-PGDS$^{-/-}$ mice exhibited more severe damage. The LPS challenge increased both the protein content of BAL fluid and the myeroperoxidase (MPO) activity of lung homogenate, an indicator of neutrophil infiltration (Fig. 1 *D* and *E*). These injury severity scores peaked by day 3 and normalized by day 10 (MPO score on day 10 WT, 42 ± 5 U/mg; H-PGDS$^{-/-}$, 64 ± 12 U/mg; n = 4 each). Both BAL protein content and MPO activity were higher in H-PGDS$^{-/-}$ mice compared with WT mice throughout the test period.

LPS inhalation increased PGD_2 production in the lungs of WT mice, peaking on day 1 (Fig. 1*F*). However, little PGD_2 production was detected in the lungs of H-PGDS$^{-/-}$ mice, suggesting that H-PGDS is a principal source of PGD_2 in this model. The foregoing observations indicate that PGD_2 is an anti-inflammatory mediator in endotoxin-induced ALI.

H-PGDS Deficiency Accelerates Fluid Accumulation, Vascular Permeability, and Cytokine Expression in Inflamed Lung. An LPS challenge induces inflammatory mediators that inhibit barrier formation of alveolar endothelial/epithelial cells. Without LPS inhalation, there was no difference between the WT and H-PGDS$^{-/-}$ mice (Fig. 2*A*). LPS inhalation slightly, but not significantly, increased the lung water content in the WT mice but caused obvious edema in the H-PGDS$^{-/-}$ mice. Dye extravasation was monitored to evaluate whether PGD_2 production can directly and acutely influence alveolar vascular permeability. In both lines of mice, the LPS challenge increased lung vascular leakage (Fig. 2 *B* and *C*). In H-PGDS$^{-/-}$ mice, much more dye was extravasated, suggesting the importance of PGD_2 in protecting the alveolar vascular barrier.

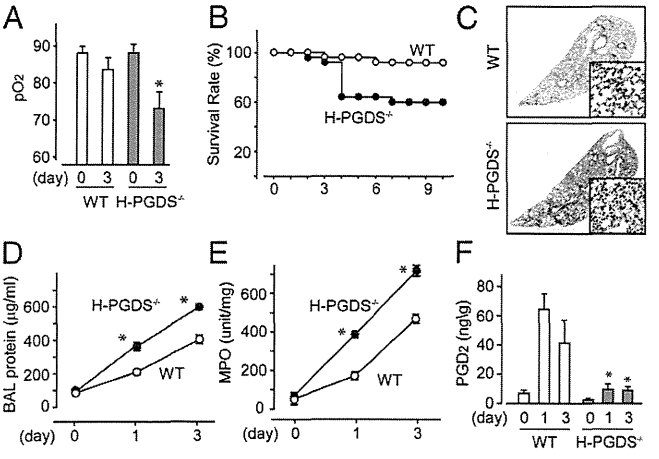

Fig. 1. H-PGDS deficiency worsens endotoxin-induced lung inflammation. (*A* and *B*) Arterial pO_2 (*A*; n = 5 each) and survival rate (*B*; n = 30 each) were monitored. (*C*) Lung morphology was examined (n = 6–8). (Scale bar: 100 μm.) (*D*) BAL fluid was collected, and protein content was measured (n = 8–9). (*E* and *F*) MPO activity (*E*) and PGD_2 content (*F*) in lung tissue homogenates were measured (*E*, n = 8 each; *F*, n = 4–5). Results are presented as the ratio of tissue dry and wet weights. *P < 0.05 compared with WT.

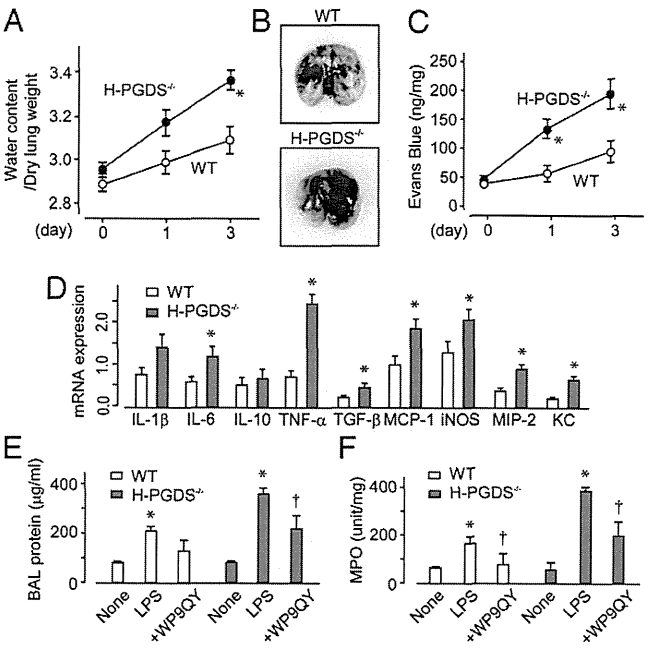

Fig. 2. H-PGDS deficiency disrupts the vascular barrier and accelerates cytokine expression in an inflamed lung. (*A*) Lung water content was calculated (n = 10–12). (*B*) On day 3, Evans blue dye was injected i.v. and circulated for 30 min. (*C*) Dye content of the lung, shown as the ratio to tissue dry weight (n = 8–10). (*D*) mRNA expression of each cytokine in LPS-treated lungs on day 1, shown as the ratio of GAPDH (n = 5 each). *P < 0.05 compared with WT. (*E* and *F*) TNF-α inhibitory peptide WP9QY was administered to the LPS-challenged mice, and the protein content in BAL fluid (*E*) and MPO activity (*F*) were measured on day 1 (n = 6 each). *,†P < 0.05 compared with nontreated and LPS-treated mice.

Quantitative RT-PCR demonstrated that the LPS challenge elevated the mRNA expression of multiple proinflammatory cytokines in the lungs of WT mice on day 1 (Fig. 2*D*). Host H-PGDS deficiency further exacerbated these results. Of particular note, TNF-α expression was elevated almost 3.3-fold in H-PGDS$^{-/-}$ mice. We previously reported that H-PGDS deficiency resulted in elevated TNF-α production, which in turn further stimulated inflammation in a tumor microenvironment (11). As expected with these observations, intranasal treatment with the TNF-α inhibitory peptide WP9QY (10 mg/kg) inhibited the inflammatory response in the H-PGDS$^{-/-}$ mice (Fig. 2 *E* and *F* and Fig. S1*A*). The enhanced inflammatory responses seen in H-PGDS$^{-/-}$ mice can be attributed, at least in part, to the increased TNF-α production.

Contribution of Hematopoietic Cell-Derived PGD_2 in Lung Inflammation. Immunostaining revealed that infiltrating Gr-1–positive neutrophils strongly expressed H-PGDS in inflamed WT mouse lung on day 3 (Fig. 3*A*, *Upper*). Platelet endothelial cell adhesion molecule (PECAM)-1–positive endothelial cells and E-cadherin–positive epithelial cells also expressed H-PGDS (Fig. 3 *B* and *C*), but at relatively low levels. No signal was detectable by anti–H-PGDS antibody in inflamed H-PGDS$^{-/-}$ lung (Fig. 3*A*, *Lower*).

Because PGD_2-mediated signaling appeared to be activated in both endothelial/epithelial cells and neutrophils, we next investigated the contributions of these two PGD_2 sources to the progression of ALI. Transplantation of H-PGDS$^{-/-}$ bone marrow (BM) exacerbated ALI, particularly in the later phase (day 3), in WT mice (compare WT+H-PGDS$^{-/-BM}$ and WT+WT^{BM}; Fig. 3*D*). Conversely, transplantation of WT^{BM} diminished later-

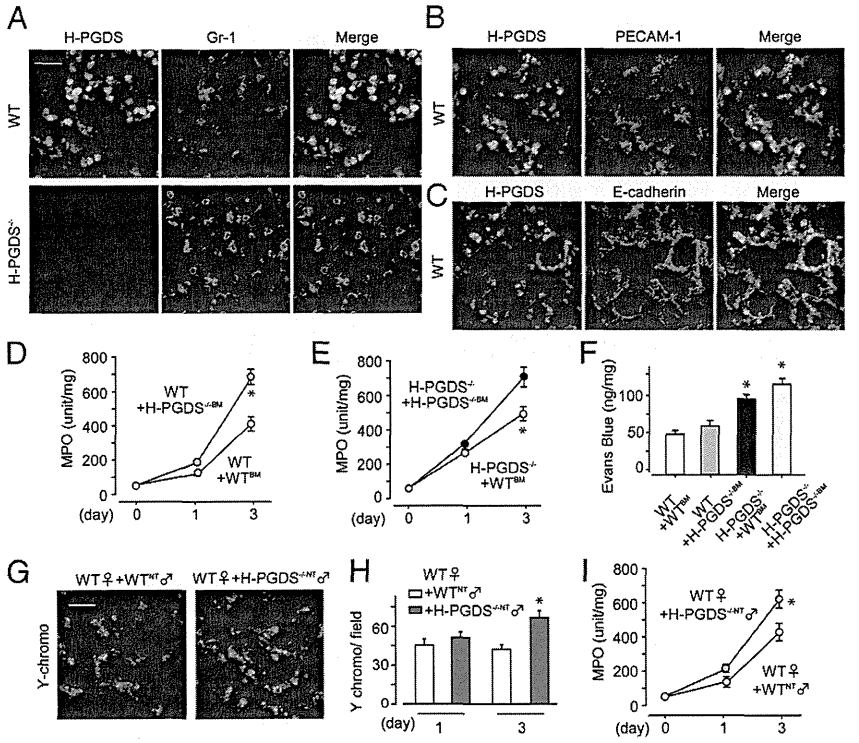

Fig. 3. Alveolar nonhematopoietic cell-derived PGD_2 contributes to form a barrier in early-phase ALI, and leukocyte-derived PGD_2 autocrinely inhibits infiltration in later-phase ALI. (*A–C*) H-PGDS expression was detected in neutrophils (*A*), endothelial cells (*B*), and epithelial cells (*C*) on day 3 ($n = 5$–6 each). (Scale bar: 50 μm.) (*D* and *E*) After bone marrow transplantation, MPO activity was measured in WT (*D*) and H-$PGDS^{-/-}$ (*E*) mice ($n = 8$ each). (*F*) Dye extravasation was monitored on day 1 ($n = 8$–10). (*G–I*) Female WT mice injected with male mouse-origin H-$PGDS^{-/-}$ or WT neutrophils were subjected to LPS inhalation. (*G*) Y chromosomes were labeled in lung sections on day 3. (Scale bar: 50 μm.) (*H*) Number of Y chromosome-positive neutrophils in fields ($n = 8$ each). (*I*) MPO activity ($n = 8$ each). $^*P < 0.05$ compared with WT +WT^{BM} (*D* and *F*), H-$PGDS^{-/-}$ +H-$PGDS^{-/-BM}$ (*E*), or WT+WT^{NT} (*H* and *I*).

phase ALI in H-$PGDS^{-/-}$ mice (compare H-$PGDS^{-/-}$+WT^{BM} and H-$PGDS^{-/-}$+H-$PGDS^{-/-BM}$; Fig. 3*E*). These findings demonstrate the importance of BM-derived hematopoietic cells, mostly neutrophils, as a functional source of PGD_2 at the progression stage of ALI. At an early phase of ALI (day 1), H-PGDS deficiency in mice of nonhematopoietic lineage (H-$PGDS^{-/-}$+WT^{BM}/H-$PGDS^{-/-}$+H-$PGDS^{-/-BM}$; Fig. 3 *D* and *E*) was associated with increased ALI scores regardless of the genotype of hematopoietic lineage cells (compare with WT+H-$PGDS^{-/-BM}$/WT+WT^{BM}). These observations show the functional impact of PGD_2 produced by nonhematopoietic alveolar cells (i.e., endothelial cells and epithelial cells) at the initiation of ALI.

We next investigated how PGD_2 derived from hematopoietic cells and PGD_2 derived from nonhematopoietic cells affect vascular barrier formation in the lung. Hematopoietic lineage-specific H-PGDS deficiency (WT+H-$PGDS^{-/-BM}$) did not substantially affect vascular permeability on day 1 (compare with WT+WT^{BM}; Fig. 3*F*), but nonhematopoietic lineage-specific H-PGDS deficiency (H-$PGDS^{-/-}$+WT^{BM}) disrupted the vascular barrier. This result suggests that PGD_2 production in cells of nonhematopoietic origin is crucial for protection of the vascular barrier in the current model of ALI.

We performed a neutrophil invasion assay to evaluate the importance of neutrophils in PGD_2-mediated immunosuppression. Neutrophils isolated from male H-$PGDS^{-/-}$ mice (H-$PGDDS^{-/-NT}$) or WT mice (WT^{NT}) were injected additively into female WT mice subjected to LPS inhalation, and infiltration of Y chromosome-positive neutrophils was assessed. During the early phases of ALI, no differences in either invasiveness (Fig. 3*H*) or MPO score (Fig. 3*I*) were detected in the two groups of mice; however, in a later phase of ALI, the H-$PGDS^{-/-NT}$ mice demonstrated a greater degree of invasiveness (Fig. 3 *G* and *H*) and thus elevated MPO scores (Fig. 3*I*). At this later phase, neutrophil-derived PGD_2 is presumed to suppress cell invasiveness following an autocrine signaling mechanism.

Roles of the PGD_2-DP and PGD_2-PGJ_2 Axes in ALI. We next investigated the involvement of each PGD receptor in PGD_2-mediated ALI suppression. In response to LPS inhalation, the lungs of DP-deficient ($DP^{-/-}$) mice, but not those of CRTH2-deficient ($CRTH2^{-/-}$) mice, demonstrated less efficient gas exchange (Fig. 4*A*), resulting in a lower survival rate (Fig. 4*B*). The lungs of $DP^{-/-}$ mice consistently showed both elevated MPO scores (Fig. 4*C*) and severe histological damage (Fig. 4*D*); however, these symptoms were still not as severe as those seen in the H-$PGDS^{-/-}$ mice (MPO score on day 3: $DP^{-/-}$, 592 ± 11; H-$PGDS^{-/-}$, 734 ± 23). This result implies a role for signal pathways other than the PGD_2-DP receptor axis in PGD_2-mediated immunosuppression.

We then investigated whether PGD_2-signal enhancement can protect against lung inflammation. In LPS-treated WT and H-$PGDS^{-/-}$ mice, intranasal administration of a DP receptor agonist, BW245C, or a degraded product of PGD_2, 15d-PGJ_2 (both at 100 μg/kg), enhanced the survival rate (Fig. 4*E*) and lowered the MPO score (Fig. 4*F*). Administration of a CRTH2 agonist DK-PGD_2 did not produce the same improvements, however.

Given that bacterial sepsis is one of the most common causes of ALI, numerous investigators have used the administration of endotoxin to initiate ALI. LPS-induced inflammatory changes are relatively mild and transient, however. In another standard model, oleic acid (OA) is used to induce ALI, which produces significantly more severe histopathological changes, similar to those observed in ARDS. In the present study, administration of OA (150 μL/kg) in addition to LPS (1.5 mg/kg) caused very severe alveolar damage. At 2 h after OA administration to WT mice, damage to the lung was characterized by extensive neutrophil infiltration, pulmonary hemorrhage (Fig. S1 *B* and *C*), respiratory dysfunction (Fig. 4*G*), and alveolar edema (Fig. 4*H*). Preadministration of either BW245C or 15d-PGJ_2 effectively diminished the injuries seen in this severe ALI/ARDS model, suggesting these agents' strong potential for therapeutic application.

Immunostaining of LPS-challenged WT mouse lung (on day 3) revealed DP-positive signals in both Gr-1–positive neutrophils (Fig. 5*A*) and PECAM-1–positive endothelial cells (Fig.

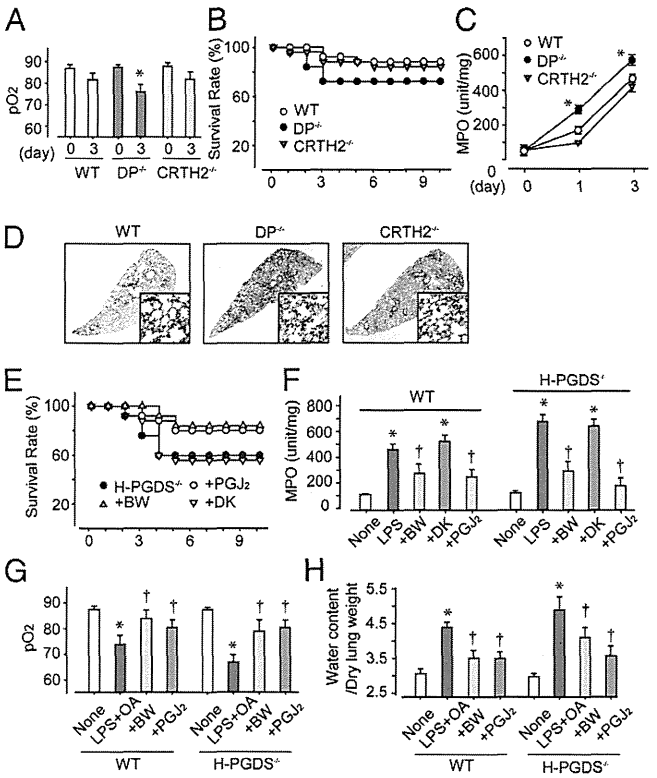

Fig. 4. (*A–D*) PGD_2-DP and PGD_2-PGJ_2 axes contribute to ALI suppression. LPS was administered to WT, $DP^{-/-}$, and $CRTH2^{-/-}$ mice, and pO_2 (*A*; $n = 5$ each), survival rate (*B*; $n = 30$ each), and MPO activity (C; $n = 8–10$ each) were monitored. (*D*) H&E staining on day 3. (Scale bar: 100 μm.) $^*P < 0.05$ compared with WT. (*E–H*) DP agonism or PGJ_2 signal enhancement is beneficial against ALI/ARDS. BW245C or 15d-PGJ_2 was administered to LPS-challenged mice and LPS+OA-challenged mice. Survival rate (*E*; $n = 25–30$) and MPO activity (*F*; $n = 8–10$) were monitored in LPS-challenged mice, and pO_2 (*G*; $n = 5$ each) and lung tissue water (*H*; $n = 8–10$) levels were monitored in LPS+OA-challenged mice at 2 h after the challenge. $^{*,\dagger}P < 0.05$ compared with LPS/LPS+OA-treated and nontreated mice.

5*B*), but not in E-cadherin–positive epithelial cells (Fig. 5*C*). These findings verify the functional contribution of DP receptors in ALI. Hematopoietic lineage-specific DP deficiency did not influence neutrophil infiltration in the WT lung (Fig. 5*D*; compared $WT+WT^{BM}$ and $WT+DP^{-/-BM}$). $DP^{-/-}+DP^{-/-BM}$ mice had significantly higher MPO scores than $WT+WT^{BM}$ mice throughout the test period. Interestingly, hematopoietic reconstitution using WT mice ($DP^{-/-}+WT^{BM}$) did not change the severity of inflammation in $DP^{-/-}$ mice (Fig. 5*E*). These findings suggest the importance of the DP-mediated signals in nonhematopoietic alveolar cells, presumably endothelial cells, in anti-inflammatory effects during ALI. In line with this idea, DP agonism was not seen in mice with a nonhematopoietic lineage-specific DP deficiency ($DP^{-/-}+WT^{BM}$) on day 3 (Fig. 5*F*). Treatment with 15d-PGJ_2 was effective regardless of the hematopoietic genotype.

We next examined the impact of DP-mediated signals on vascular barrier formation and neutrophil motility. On a dye extravasation assay, mice lacking DP from a nonhematopoietic lineage ($DP^{-/-}+WT^{BM}$ and $DP^{-/-}+DP^{-/-BM}$) exhibited defective vascular barrier formation on day 3 regardless of hematopoietic genotype (Fig. 5*G*). As demonstrated by the neutrophil infiltration assay, DP deficiency in the neutrophils of LPS-challenged WT mice did not affect the infiltrative capability of these cells on day 3 (Fig. 5*H*). This finding reinforces the crucial role of the PGD_2-DP signal axis in nonhematopoietic alveolar cells in protecting the vascular barrier against inflammation.

DP Agonist, But Not PGJ_2, Inhibits Vascular Permeability in Vitro. ALI progression has three main phases: cytokine expression, vascular barrier disruption, and neutrophil infiltration. In vitro LPS treatment (50 ng/mL for 6 h) of both WT and H-$PGDS^{-/-}$ mouse lung endothelial cells (MLECs) resulted in elevated mRNA expression of TNF-α (Fig. 6*A*). In line with the in vivo data, H-$PGDS^{-/-}$ MLECs were more responsive to LPS challenge compared with WT MLECs. Pretreatment with DP agonist BW245C (0.3 μM) or 15d-PGJ_2 (0.3 μM) attenuated the elevated gene expression of TNF-α in both MLEC lines.

Treatment with PGD_2 (1–3 μM) or the DP agonist BW245C (0.1–0.3 μM) increased transendothelial electrical resistance (TER), indicating decreased permeability in human pulmonary arterial endothelial cells (Fig. 6 *B* and *C*). Consistent with our previous study showing that DP agonism tightens the endothelial barrier through cAMP–protein kinase A activation in bovine aortic endothelial cells (10), treatment with the cAMP booster forskolin (1 μM) enhanced endothelial barrier formation. In contrast, treatment with the CRTH2 agonist DK-PGD_2 (0.3–1 μM) or 15d-PGJ_2 (0.3–1 μM) did not affect endothelial barrier formation in vitro.

In the transmembrane migration assay, isolated neutrophils migrated toward a solution of 10 nM leukotriene B_4 (LTB_4) added to the lower chamber (Fig. 6*D*). The addition of 15d-PGJ_2 (1 μM) significantly inhibited LTB_4-induced neutrophil migration, with no agonism resulting from the addition of BW245C (0.3 μM) or DK-PGD_2 (1 μM).

The foregoing in vitro experiments suggest that PGD_2 plays an anti-inflammatory role in ALI through either of two different signaling pathways: DP-dependent or PGJ_2-dependent. The DP-mediated signaling is found mainly in endothelial cells, whereas PGJ_2-mediated signaling is seen in various other cell types.

Discussion

The main purpose of the present study was to define the roles of PGD_2-mediated signals in the pathogenesis of ALI, focusing on its producer–effector interaction in vivo. We have demonstrated that the functional source of PGD_2 shifts from alveolar endothelial/epithelial cells to infiltrating neutrophils along with ALI progression, and that the PGD_2 thus produced represents an anti-inflammatory response through DP-mediated signaling arising mainly in endothelial cells and PGJ_2 signaling in various other types of cells (Fig. S2).

PGs play paradoxical roles, both proinflammatory and anti-inflammatory, in injured lungs (12). Major PGs, including thromboxane A_2 (TXA_2) and PGE_2, are classified mostly as proinflammatory PGs in ALI. Treatment with TXA_2 synthase inhibitor or gene deficiency of PGE receptor EP3 has been found to attenuate lung edema in mice (13, 14). In contrast, anti-inflammatory roles for lipoxin A_4 and 15d-PGJ_2 have been reported in mouse ALI models (15, 16). Apparently, ALI induction is intricately modulated by a variety of PGs. Given that the pathophysiological action of each PG varies with its engaged receptor subtypes, target cells, and context of activation, a detailed evaluation of the role of each PG with respect to its source and effector is indispensable to unraveling this complexity and ultimately overcoming ALI.

Our observations consistently demonstrate the anti-inflammatory effects of PGD_2, as well as the related therapeutic potential of DP agonism and PGJ_2 treatment in ALI/ARDS models. Some previous studies have suggested a proinflammatory role for PGD_2 in certain respiratory disorders, with the mechanisms mediated through signaling pathways other than those that we have studied here. Monneret et al. (17) reported that PGD_2 inhalation caused bronchoconstriction by cross-reacting with the

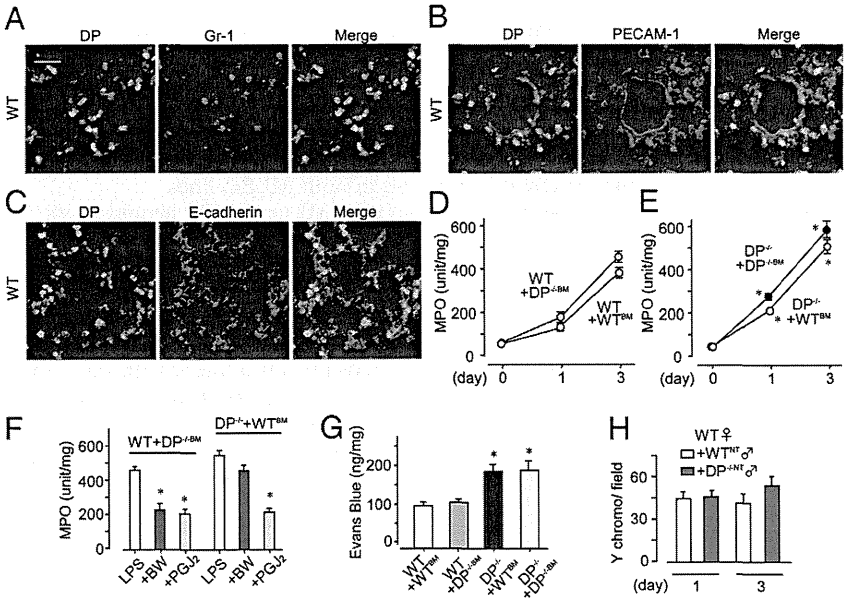

Fig. 5. DP activation in endothelial cells is beneficial against ALI. (*A–C*) DP protein expression was detected in neutrophils (*A*) and endothelial cells (*B*), but not in epithelial cells (*C*), on day 3 ($n = 5$ each). (Scale bar: 50 μm.) (*D* and *E*) After bone marrow transplantation, MPO activity was monitored in WT, $DP^{-/-}$, and $CRTH2^{+}$ mice ($n = 8$ each). (*F* and *G*) BW245C or 15d-PGJ_2 was administered to LPS-challenged mice, and MPO activity (*F*; $n = 6–8$) and dye extravasation (*G*; $n = 6–8$) were monitored on day 3. (*H*) The infiltrating ability of $DP^{-/-}$ neutrophils isolated from male mice into inflamed WT lung was monitored on day 3 ($n = 8$ each). $^{*,\dagger}P < 0.05$ compared with WT+WT^{BM} (*E*), LPS-treated (*F*), and WT+WT^{NT} (*G*) mice.

TXA_2 receptor TP. Another group reported that PGD_2 causes eosinophil and basophil chemotaxis by interacting with a CRTH2 receptor (7). Like the other PGs, PGD_2 appears to have a dual role, tissue-protective or tissue-invasive in the context of airway inflammation. This action may depend on the specific receptor involved, the specific type of pathogenesis occurring, and the severity and stage of the disease.

Clearly identifying the types of cells playing the greatest roles in the responses to these related respiratory pathologies is difficult, particularly in vivo. We found that hematopoietic replacement allowed us to determine the active histocellular site of PGD_2 signaling in the ALI model. Using this procedure, we determined that the PGD_2-DP signaling arising in lung cells of nonhematopoietic origin (i.e., endothelial/epithelial cells) is responsible for the anti-inflammatory response in early stages of ALI (Figs. 3 *D–F* and 5 *D–G*). In contrast, PGD_2 produced by hematopoietic origin, most likely neutrophils, play a central role in the immunosuppressive response in the later stages of ALI. As an effector signal, the DP-mediated anti-inflammatory response of native resident lung cells is involved in all phases of ALI. Given the strong links among vascular permeability, immune cell infiltration, and cytokine induction, determining the specific contributions of DP-mediated anti-inflammatory reactions in vivo is difficult. However, our data derived from both dye extravasation experiments (Fig. 5*G*) and in vitro experiments clearly indicate that PGD_2-DP signaling acutely and directly inhibited alveolar vascular permeability (Fig. 6 *B* and *C*). Furthermore, we found that DP-stimulation targeting mainly to endothelial cells strongly inhibited the symptoms of ALI (Fig. 5*F*). Teijaro et al. (18) recently reported that a proinflammatory cytokine burst in vascular endothelial cells is the major factor promoting infection-induced ALI. Although detailed investigations are needed to clarify the contributions of PGD_2 signaling to epithelial immune responses, the application of endothelial suppressants might be a rational strategy against ALI/ARDS.

In the present study, H-PGDS deficiency enhanced the inflammatory response to a much greater degree than DP deficiency, suggesting the existence of an alternative signaling pathway in addition to the DP-mediated pathway. Lipoxins are anti-inflammatory lipid mediators that potently inhibit neutrophil infiltration (19). In preliminary experiments, we investigated the possibility that PGD_2 produces an anti-inflammatory reaction by stimulating lipoxin production, but detected no definite correlation between these two mediators (Fig. S3 *A–D*). It is also well known that a degraded product of PGD_2, 15d-PGJ_2, exerts anti-inflammatory effects through either a PPAR-γ–dependent pathway or a PPAR-γ–independent pathway. We have shown here that administration of 15d-PGJ_2 produces a therapeutic action against ALI/ARDS in vivo (Fig. 4 *E–H*). Our in vitro experiments suggest that 15d-PGJ_2–mediated suppression of both cytokine expression and neutrophil migration contribute to this action (Fig. 6 *A* and *D*). Genovese et al. (20) reported that administration of the PPAR-γ agonist rosiglitazone or 15d-PGJ_2 moderates bleomycin-induced mouse lung injury. Another group demonstrated that 15d-PGJ_2 is protective against carrageenan-induced ALI through a nuclear factor erythroid 2-related factor-2 (Nrf-2)-mediated transcriptional pathway (16). Rajakariar et al. (21) reported that 15d-PGJ_2 is produced at sufficient levels in vivo to drive the resolution of zymosan-induced mouse peritonitis.

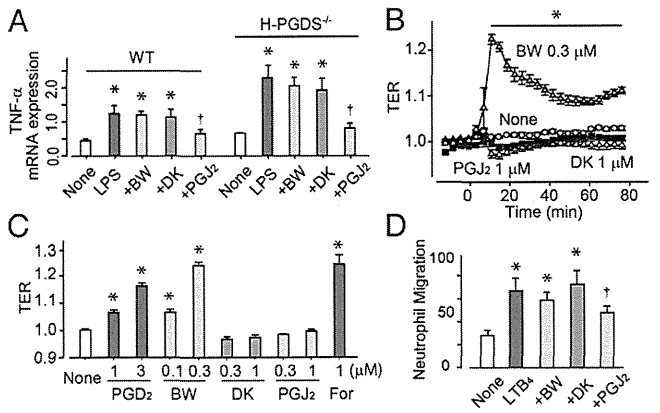

Fig. 6. PGJ_2 signal inhibits cytokine expression in endothelial cells and neutrophil migration, and DP agonism enhances endothelial barrier formation. (*A*) mRNA expression of TNF-α in mouse lung endothelial cells, shown as the ratio of GAPDH ($n = 5$ each). (*B* and *C*) TER; typical responses are shown in *B*, and data are summarized in *C* ($n = 4–6$). (*D*) Transmembrane migration assay performed using isolated neutrophils. LTB_4 was added to the lower chamber and test agents were added to both the lower and upper chambers. Data represent the number of migrating cells to lower chambers in one field (20×; $n = 5$ each). $^{*,\dagger}P < 0.05$ compared with nontreated or LPS-treated cells.

Thus, PGD_2 may produce an anti-inflammatory effect in ALI, in part through PGJ_2-dependent signaling pathways.

In summary, PGD_2 is an anti-inflammatory mediator in endotoxin-induced ALI, and enhancing its signal can be beneficial in the treatment of ALI/ARDS. The site of PGD_2 activity shifts from native lung resident cells to infiltrating immune cells during the pathological progression of ALI.

Materials and Methods

Experimental Animals and ALI Induction. All experiments were approved by the University of Tokyo's Institutional Animal Care and Use Committee. H-PGDS$^{-/-}$, DP$^{-/-}$, and CRTH2$^{-/-}$ mice (C57BL/6) were generated and bred as described previously (22–24). For BM transplantation, 5-wk-old female mice received 9 Gy irradiation for BM ablation. BM cells (2×10^6) freshly isolated from donor mice were injected into the tail vein of the recipient. The mice were used for the experiments at 6 wk after transplantation.

To induce ALI, female mice (25 g) were anesthetized with 1.5% isoflurane, and *Escherichia coli* endotoxin LPS (O55:B5; 3.75 mg/kg) was instilled intratracheally. Intranasal administration of WP9QY (10 mg/kg), BW245C (100 μg/kg), DK-PGD_2 (100 μg/kg), or 15d-PGJ_2 (100 μg/kg) was started 10 min before the LPS challenge and then repeated every 3 h for WP9QY or every 12 h for the other agents. OA (0.15 mL/kg) was administered i.v. at 30 min after the instillation of LPS (1.5 mg/kg) to provoke severe inflammation.

Analysis of BAL Fluid, Blood Gases, and Lung Edema. BAL was collected by flushing the lung with 1 mL of saline solution although a tracheal annula. Protein concentrations in BAL were measured. For blood gas measurements, blood drawn from the abdominal aorta was analyzed with an i-STAT blood analyzer (FUSO Pharmaceutical Industries) following the manufacturer's instructions.

To measure lung water content, the excised lungs were weighed, then dried and reweighed. Water content was calculated by subtracting the dry weight from the wet weight. For permeability assessment, Evans blue dye (30 mg/kg) was injected i.v. and circulated for 3 h. Mice were killed and perfused with saline solution. Extravasated dye into lung tissue was extracted in formamide, and the contents were quantified spectrophotometrically.

PGD_2 Measurement and MPO Assay. Dissected lungs were homogenized in ethanol containing 0.02% HCl, and the samples were separated by HPLC. MS was performed using an API 3200 triple-quadruple tandem mass spectrometer (AB SCIEX). For MPO assays, dissected lungs were homogenized in potassium phosphate buffer containing 0.3% hexadecyltrimenthyl ammonium bromide. After centrifugation, supernatant was collected. Then 0.5 mM o-dianisidine dihydrochloride (MP Biochemicals) and 0.05% hydrogen peroxide were added to the supernatant, and optical density was measured at 460 nm.

Morphological Studies. Paraffin-embedded sections (4 μm) were used for H&E staining. Cryosections (5 μm) were used for all other stainings. Primary antibodies included anti–H-PGDS, DP (Cayman Chemicals), anti–Gr-1, anti-CD31, and anti–E-cadherin (BD Biosciences) antibodies. In some experiments, cryosections were labeled with biotin-labeled DNA probes against the Y chromosome (Chromosome Science), following the manufacturer's protocol.

Isolation of MLECs and Quantitative RT-PCR. Lung tissue was dissected, minced in 0.1% collagenase, and homogenized. Magnetic beads (Dynal) coated with anti–ICAM-2 antibodies (BD Pharmingen) were added to the cells. After a 1-h incubation, endothelial cells were collected using a magnetic holder, washed, and plated and passaged for use. After 48 h, serum-starved endothelial cells were used for experiments.

Total RNA was isolated and reverse-transcribed into cDNA. Subsequent quantitative PCR using platinum SYBR Green qPCR SuperMix-UDG (Invitrogen) and specific primers was performed with an ABI Prism 7000 (Applied Biosystems).

TER Measurement. Endothelial barrier integrity was evaluated by measuring TER using an Xcelligence real-time cell analyzer DP system (Roche). In brief, human pulmonary arterial endothelial cells were seeded on gold electrodes and incubated overnight, after which electrical resistance across the cell layer was determined. The TER value thus derived was divided by the initial value for normalization.

Isolation of Neutrophil and Chemotaxis Assay. Marrow cavities of the tibias and femurs of 8-wk-old mice were flushed with DMEM with 10% FCS. Neutrophils were isolated by centrifugation over discontinuous Percoll gradients. For neutrophil invasion assays, 5×10^6 neutrophils were injected into tail veins of recipient mice each day.

A modified Boyden chamber with 8-μm pores (BD Biosciences) was used for chemotaxis assays. Stimulants were added to the bottom chamber, and inhibitors were added to both the upper and bottom chambers. Isolated neutrophils (2×10^5 cells) were applied to the upper chambers. After 1 h, cells on the membrane were fixed and stained with Giemsa solution. The number of cells from five randomly chosen fields (200×) on the lower side of the membrane was counted.

Statistical Analyses. All data are presented as mean ± SEM. Statistical differences were determined using the Student *t* test for two-group comparisons and one-way ANOVA with Dunnett's test for multiple-group comparisons.

ACKNOWLEDGMENTS. This work was supported by a Grant-in-Aid for Young Scientists (A) and a Grant-in-Aid for Challenging Exploratory Research from the Ministry of Education, Culture, Sports, Science and Technology, and by the Japan Society for the Promotion of Science, Takeda Science Foundation, and Pharmacological Research Foundation, Tokyo.

1. Ware LB, Matthay MA (2000) The acute respiratory distress syndrome. *N Engl J Med* 342(18):1334–1349.
2. Frank JA, Matthay MA (2005) Leukotrienes in acute lung injury: A potential therapeutic target? *Am J Respir Crit Care Med* 172(3):261–262.
3. Hinshaw LB, Solomon LA, Erdös EG, Reins DA, Gunter BJ (1967) Effects of acetylsalicylic acid on the canine response to endotoxin. *J Pharmacol Exp Ther* 157(3):665–671.
4. Cuzzocrea S, et al. (2002) Protective effects of Celecoxib on lung injury and red blood cells modification induced by carrageenan in the rat. *Biochem Pharmacol* 63(4): 785–795.
5. Bernard GR, et al.; The Ibuprofen in Sepsis Study Group (1997) The effects of ibuprofen on the physiology and survival of patients with sepsis. *N Engl J Med* 336(13): 912–918.
6. Kostenis E, Ulven T (2006) Emerging roles of DP and CRTH2 in allergic inflammation. *Trends Mol Med* 12(4):148–158.
7. Hirai H, et al. (2001) Prostaglandin D_2 selectively induces chemotaxis in T helper type 2 cells, eosinophils, and basophils via seven-transmembrane receptor CRTH2. *J Exp Med* 193(2):255–261.
8. Honda K, et al. (2003) Prostaglandin D_2 reinforces Th2 type inflammatory responses of airways to low-dose antigen through bronchial expression of macrophage-derived chemokine. *J Exp Med* 198(4):533–543.
9. Scher JU, Pillinger MH (2005) 15d-PGJ_2: The anti-inflammatory prostaglandin? *Clin Immunol* 114(2):100–109.
10. Murata T, et al. (2008) Role of prostaglandin D_2 receptor DP as a suppressor of tumor hyperpermeability and angiogenesis in vivo. *Proc Natl Acad Sci USA* 105(50): 20009–20014.
11. Murata T, et al. (2011) Prostagladin D_2 is a mast cell-derived antiangiogenic factor in lung carcinoma. *Proc Natl Acad Sci USA* 108(49):19802–19807.
12. Gilroy DW, et al. (1999) Inducible cyclooxygenase may have anti-inflammatory properties. *Nat Med* 5(6):698–701.
13. Ishitsuka Y, et al. (2004) Involvement of thromboxane A_2 (TXA_2) in the early stages of oleic acid-induced lung injury and the preventive effect of ozagrel, a TXA_2 synthase inhibitor, in guinea-pigs. *J Pharm Pharmacol* 56(4):513–520.
14. Göggel R, Hoffman S, Nüsing R, Narumiya S, Uhlig S (2002) Platelet-activating factor-induced pulmonary edema is partly mediated by prostaglandin E(2), E-prostanoid 3-receptors, and potassium channels. *Am J Respir Crit Care Med* 166(5):657–662.
15. Fukunaga K, Kohli P, Bonnans C, Fredenburgh LE, Levy BD (2005) Cyclooxygenase 2 plays a pivotal role in the resolution of acute lung injury. *J Immunol* 174(8):5033–5039.
16. Mochizuki M, et al. (2005) Role of 15-deoxy delta(12,14) prostaglandin J_2 and Nrf2 pathways in protection against acute lung injury. *Am J Respir Crit Care Med* 171(11): 1260–1266.
17. Spik I, et al. (2005) Activation of the prostaglandin D_2 receptor DP2/CRTH2 increases allergic inflammation in mouse. *J Immunol* 174(6):3703–3708.
18. Teijaro JR, et al. (2011) Endothelial cells are central orchestrators of cytokine amplification during influenza virus infection. *Cell* 146(6):980–991.
19. Levy BD, Clish CB, Schmidt B, Gronert K, Serhan CN (2001) Lipid mediator class switching during acute inflammation: Signals in resolution. *Nat Immunol* 2(7): 612–619.
20. Genovese T, et al. (2005) Effect of rosiglitazone and 15-deoxy-Delta^{12,14}-prostaglandin J_2 on bleomycin-induced lung injury. *Eur Respir J* 25(2):225–234.
21. Rajakariar R, et al. (2007) Hematopoietic prostaglandin D2 synthase controls the onset and resolution of acute inflammation through PGD_2 and 15-deoxyDelta$^{12\ 14}$ PGJ_2. *Proc Natl Acad Sci USA* 104(52):20979–20984.
22. Matsuoka T, et al. (2000) Prostaglandin D_2 as a mediator of allergic asthma. *Science* 287(5460):2013–2017.
23. Mohri I, et al. (2006) Prostaglandin D_2-mediated microglia/astrocyte interaction enhances astrogliosis and demyelination in twitcher. *J Neurosci* 26(16):4383–4393.
24. Satoh T, et al. (2006) Prostaglandin D_2 plays an essential role in chronic allergic inflammation of the skin via CRTH2 receptor. *J Immunol* 177(4):2621–2629.